Title: Hepatic γ-Amino Butyric Acid Release Drives Hyperinsulinemia and Insulin Resistance

Authors: Caroline. E. Geisler[1], Susma. Ghimire[1], Chelsea. Hepler[1,2], Mark. R. Higgins[1], Ralph. F. Fregosi[3], Benjamin. J. Renquist[1]*

Affiliations:

[1]School of Animal and Comparative Biomedical Sciences, University of Arizona, Tucson, AZ 85721 USA.

[2]Robert H. Lurie Medical Research Center, Northwestern University, Chicago , IL 60611 USA.

[3]Department of Physiology, University of Arizona, Tucson, AZ 85721 USA.

*To whom correspondence should be addressed. bjrenquist@email.arizona.edu

Competing Interests: The results presented in this paper have resulted in patent cooperation treaty Application No. 62/511,753 and 62/647,468: METHODS AND COMPOSITIONS FOR REGULATING GLUCOSE HOMEOSTASIS.

Abstract

The degree of hepatic lipid accumulation in obesity directly correlates with the severity of hyperinsulinemia and systemic insulin resistance. Here, we propose a mechanism that explains this associative link, whereby, hepatic steatosis dysregulates glucose and insulin homeostasis. Obesity-induced lipid accumulation results in hepatocyte depolarization. We have established that hepatocyte depolarization depresses hepatic afferent vagal nerve firing and diet induced obesity increases hepatic GABA release in mice. Hepatic GABA release decreases hepatic afferent vagal nerve activity to stimulate pancreatic insulin release and decreases insulin sensitivity. Surgically eliminating the hepatic vagal nerve signaling, preventing hepatic GABA synthesis, or limiting hepatic GABA export ameliorates hyperinsulinemia and insulin resistance in diet-induced obese mice. This work establishes that limiting hepatocyte GABA production or release may mute the glucoregulatory dysfunction common to obesity.

Keywords: Obesity, NAFLD, NASH, Hyperinsulinemia, Insulin Resistance, GABA, GABA Transaminase, Aspartate

Introduction

Type II diabetes (T2D) is a global health concern that affects 30 million Americans, doubling both the risk of death and medical costs for an individual (1). Non-alcoholic fatty liver disease (NAFLD) is strongly associated with an increased risk of developing diabetes, while the degree of hepatic steatosis is directly related to the severity of systemic insulin resistance, glucose intolerance, and hyperinsulinemia (2-4). We aimed to identify the mechanism by which hepatic lipid accumulation induces hyperinsulinemia and insulin resistance.

The hepatic vagal nerve acts as a conduit by which the liver communicates nutritional status to affect pancreatic insulin release and peripheral tissue insulin sensitivity. A decrease in HVAN firing frequency stimulates insulin release, while conversely an increase in HVAN firing frequency decreases serum insulin (5, 6). The HVAN also regulates whole-body insulin sensitivity. Hepatic vagotomy diminishes insulin sensitivity and skeletal muscle glucose clearance in insulin sensitive rats, while improving insulin sensitivity and glucose tolerance in insulin resistant mice (7, 8). Therefore, the firing frequency of the HVAN is integral to controlling insulin secretion and sensitivity.

Hepatic lipid accumulation depolarizes hepatocytes (9). Because NAFLD is integral to the development of hyperinsulinemia and insulin resistance and the HVAN regulates insulin secretion and action, we tested the hypothesis that lipid induced hepatocyte depolarization alters firing activity of the HVAN to drive the dysregulation of systemic glucose homeostasis common in obesity.

Results

Hepatic Vagotomy Protects Against Diet-Induced Hyperinsulinemia

To investigate our hypothesis that hepatic lipid accumulation drives hyperinsulinemia and insulin resistance by altering HVAN activity, we set out to test if obesity induced insulin dysregulation is dependent on an intact hepatic vagal nerve. We hypothesized that hepatic vagotomy would mute obesity induced hyperinsulinemia and insulin resistance. We performed hepatic vagotomy or sham surgery in lean mice then provided them a 60% high fat diet (HFD; Teklad, TD 06414) for 9 weeks. Vagotomy did not significantly affect weight gain on a HFD (Fig. 1A). Hepatic vagotomy lowered serum insulin at 9 weeks of HFD feeding and elevated the glucose:insulin ratio at both 0 and at 9 weeks on the HFD, without affecting serum glucose concentrations (Fig. 1B-1D). For the same increase in body weight during HFD feeding, the rise in serum insulin was greater in sham than vagotomized mice (Fig. 1E). Hepatic vagotomy also tended to decrease serum glucagon in HFD fed mice ($P < 0.07$; Fig. 1F).

Vagotomy improved oral glucose tolerance at 9 weeks on the HFD, while simultaneously decreasing glucose stimulated insulin concentrations (Figs. 1G-1I). Vagotomy tended to improve insulin sensitivity in HFD induced obese mice (Figs. 1J-1K). These data support the conclusion that surgically interrupting hepatic vagal signaling attenuates the development of diet-induced hyperinsulinemia and glucose intolerance.

Hepatocyte Depolarization Depresses HVAN Firing Activity

Obesity depolarizes hepatocytes (Fig. 2A). We hypothesize that obesity induced hepatocyte depolarization is communicated through the HVAN to dysregulate insulin secretion and action. We used the genetically-engineered, PSEM89S ligand-gated depolarizing ion channel described by Magnus, et al. (2011), to assess the effect of hepatocyte depolarization on HVAN firing activity (10). We intravenously delivered an adeno-associated virus serotype 8 (AAV8) encoding this PSEM89S ligand-gated depolarizing channel and green fluorescent protein (eGFP) flanked by LoxP sites to wildtype mice or mice expressing

liver specific cre-recombinase driven by the albumin promoter (11, 12). Thus, this channel will only be expressed in albumin-cre recombinase expressing mice and only in the presence of PSEM89S ligand will hepatocytes be depolarized. We performed immunohistochemistry against GFP to confirm liver specific channel expression in albumin-cre expressing mice and no expression in wildtype mice (Supplemental Figs. 1A-1B). No GFP expression was observed in skeletal muscle, pancreas, or adipose tissue of albumin-cre mice (Supplemental Fig. 1C). To assess the influence of hepatocyte depolarization on HVAN firing activity we simultaneously measured hepatocyte membrane potential and HVAN activity in the anesthetized mouse. Bath application of the PSEM89S ligand (30 μM) depolarized hepatocytes and decreased HVAN firing activity in albumin-cre, channel expressing mice (Figs. 2B-2C), while having no effect on either hepatocyte membrane potential or HVAN in wildtype mice (Figs. 2B-2C).

Acute Hepatic Depolarization Elevates Serum insulin

Hepatocyte depolarization depresses HVAN activity (Figs. 2B-2C), while loss of HVAN signaling in obesity protects against the development of hyperinsulinemia (Fig. 1B). Therefore, we hypothesize that hepatocyte depolarization causes hyperinsulinemia. To directly test this causative relationship, we assessed the insulin response to PSEM89S ligand-induced hepatocyte depolarization. Intraperitoneal administration of PSEM89S ligand (30 mg/kg) more than doubled serum insulin and decreased serum glucose concentrations in albumin-cre mice, whose hepatocytes express the PSEM89S ligand activated depolarizing channel (Figs. 2D-2E). Accordingly, PSEM89S ligand decreased the glucose:insulin ratio in albumin-cre mice (Fig. 2F). Notably, PSEM89S ligand did not alter serum insulin, glucose, or the glucose:insulin ratio in wildtype mice (Figs. 2D-2F).

We developed a second model of hepatocyte depolarization in which liver specific expression of the same PSEM89S ligand-gated depolarizing channel and GFP was independent of cre-recombinase and instead driven by the liver specific thyroxine binding globulin (TBG) promoter (13, 14). Wildtype mice intravenously injected with this AAV8 had liver specific GFP expression that was confirmed by immunohistochemistry (Supplemental Fig. 1D). No GFP expression was observed in skeletal muscle,

pancreas, or adipose tissue (Supplemental Fig. 1E). To ensure stimulatory concentrations of circulating glucose, we gave an oral glucose gavage (2.5 g/kg body weight) 10 minutes following IP PSEM89S ligand (30 mg/kg) injection. As previously observed, intraperitoneal PSEM89S ligand administration elevated serum insulin and lowered the glucose:insulin ratio in mice expressing the depolarizing channel (Figs. 1G and 1I). PSEM89S ligand injection did not affect the rise in serum glucose following an oral gavage of glucose (Fig. 1H). These data establish that acute hepatocyte depolarization depresses HVAN firing activity and increases serum insulin concentrations.

Hepatic Hyperpolarization Protects Against Diet-Induced Metabolic Dysfunction

Having established that hepatocyte depolarization increases serum insulin concentrations (Fig. 2), and that the hepatic vagal nerve is essential for diet induced hyperinsulinemia (Fig. 1B), we next hypothesized that hepatocyte hyperpolarization would prevent obesity induced hyperinsulinemia. To induce a chronic hyperpolarized state, we used an AAV8 viral vector encoding TBG promoter driven expression of the inward rectifying K^+ channel, Kir2.1, and eGFP (Fig. 3A). Although this channel is inwardly rectifying in neurons, in hepatocytes, with a resting membrane potential that ranges from -20 to -50 mV, Kir2.1 channel expression supports K^+ efflux and hyperpolarization (15). We confirmed the hyperpolarizing effect of Kir2.1 by *in vivo* intracellular measurement of the membrane potential of hepatocytes before and after bath application of the Kir2.1 antagonist, Barium (Ba^{2+}; 50 μM) (15). Ba^{2+} induced a 6.86±1.54 mV depolarization of hepatocytes in Kir2.1 expressing mice but had no effect (-0.62±1.86 mV) in control eGFP expressing mice (Fig. 3B).

In lean mice, hepatocyte hyperpolarization decreased basal serum insulin and glucose concentrations (Supplemental Figs. 2A-2C), improved glucose clearance (Supplemental Figs. 2D-2F) and enhanced insulin sensitivity (Supplemental Figs. 2G-2H). Kir2.1 expression did not affect gluconeogenic potential, as assessed by a pyruvate tolerance test (Supplemental Figs. 2I-2J). This establishes that hepatocyte membrane potential regulates systemic glucose homeostasis in non-disease conditions.

Kir2.1 and eGFP expressing mice were provided a HFD for 9 weeks. Kir2.1 expression depressed weight gain on a HFD, reaching significance from weeks 6-9 on the HFD (Fig. 3C). Kir2.1 expression limited the rise in serum insulin and glucose in response to 3, 6, or 9 weeks of HFD feeding, and increased the glucose:insulin ratio after 9 weeks on the HFD (Figs. 3D-3F). Although Kir2.1 expression limited HFD induced weight gain, the same increase in body weight led to a greater increase in serum insulin concentration in eGFP control than in Kir2.1 expressing mice (Fig. 3G). Given the key anabolic role of insulin signaling (16, 17), the depressed HFD induced weight gain in Kir2.1 expressing mice may be secondary to the decreased serum insulin. Importantly, Kir2.1 expression did not affect HFD induced hepatic lipid accumulation (Kir2.1: 94.2±10.6 mg triglycerides/g liver versus eGFP control: 98.4±6.6 mg triglycerides/g liver; $P = 0.73$). The absence of hyperinsulinemia in obese Kir2.1 expressing mice despite the development of hepatic steatosis supports hepatocyte depolarization as a critical mediator in the relationship between hepatic lipid accumulation and dysregulated glucose homeostasis. Kir2.1 expression decreased serum glucagon in diet induced obese mice (Fig. 3H).

At 3 weeks on the HFD, Kir2.1 expression improved glucose clearance without altering glucose stimulated serum insulin (Supplemental Figs. 3A-3C). Kir2.1 expression tended to improved insulin sensitivity at 3 weeks of HFD feeding ($P = 0.064$; Supplemental Figs. 3D-3E). After 9 weeks on the HFD, Kir2.1 expression improved glucose tolerance and insulin sensitivity (Figs. 3I-3M), while having no effect on gluconeogenic potential from pyruvate (Figs. 3N-3O). These results support the proposition that hepatocyte hyperpolarization protects against the development of hyperinsulinemia, hyperglucagonemia, hyperglycemia, glucose intolerance, and insulin resistance in diet induced obesity.

Obesity Alters Hepatocyte Neurotransmitter Production, while Membrane Potential Affects Neurotransmitter Release

Resolving the mechanism by which hepatocyte membrane potential can alter HVAN and downstream peripheral nervous system activity is critical to understanding the link between fatty liver and insulin dysregulation. To investigate the possibility that the liver releases neurotransmitters to affect HVAN

firing activity, we incubated liver slices *ex vivo* and measured the release of neurotransmitters into the media (Supplemental Table 1).

Since obesity depolarizes hepatocytes (Fig. 2A), and hepatocyte depolarization decreases HVAN firing activity (Figs. 2B-2C), we hypothesized that obese livers would display either an increase in the release of inhibitory or a decrease in the release of excitatory neurotransmitters. Liver slices from obese mice released more of the inhibitory neurotransmitter GABA than liver slices from lean mice (Fig. 4A). Hepatocytes synthesize GABA via the mitochondrial enzyme GABA-Transaminase (GABA-T) (18). Hepatic GABA-T mRNA expression is increased in diet induced obesity (Fig. 4B).

Hepatic GABA transporters, Betaine GABA transporter 1 (BGT1) and GABA transporter 2 (GAT2), both co-transport 3 sodium ions and 1 chloride ion (19). To establish the role of these ion dependent transporters in GABA export we show that hepatic slice GABA release is encouraged by incubation in media with low concentrations of sodium and chloride ions (Fig. 4C). Diet induced obesity decreases hepatic ATP concentrations (Fig. 4D) and lowers hepatic activity of the Na^+/K^+ ATPase (20). We propose that increased intracellular sodium ions and hepatocyte depolarization resulting from diminished Na^+/K^+ ATPase activity in obesity promotes GABA efflux (Fig. 4G).

Kir2.1 expression decreased obesity induced hepatocyte slice GABA release without altering the obesity induced increase in GABA-T mRNA expression (Figs. 4A-4B). The electrogenic nature of GABA transporters results in GABA export being stimulated by hepatocyte depolarization and inhibited by hepatocyte hyperpolarization. In turn, preventing obesity induced hepatocyte depolarization through viral induced Kir2.1 expression decreases GABA export (Fig. 4G).

To establish the relationship between GABA-T activity and hepatocyte GABA release, we treated liver slices with the irreversible GABA-T inhibitor, ethanolamine-O-sulphate *ex vivo* (EOS; 5.3 mM). GABA-T inhibition decreased GABA export from obese control and obese Kir2.1 expressing liver slices, but not liver slices from lean mice (Fig. 4E). This supports the hypothesis that GABA production is elevated

in obesity and that GABA-T mediated synthesis of GABA is not impaired by Kir2.1 expression. Hepatocytes from obese mice also released less of the excitatory neurotransmitter, aspartate, than hepatocytes from lean mice (Fig. 4F). Although Kir2.1 decreased GABA release, there was no effect of Kir2.1 expression on the obesity induced decrease in aspartate release from liver slices (Fig. 4F).

GABA-Transaminase Inhibition Improves Glucose Homeostasis in Obesity

To directly assess the effect of GABA-T in obesity-induced insulin resistance, hyperinsulinemia, and hyperglycemia, we treated obese mice with either EOS or a second irreversible GABA-T inhibitor, vigabatrin (8 mg/day), both reduce hepatic GABA-T activity by over 90% within two days (21). EOS does not readily cross the blood brain barrier or decrease central nervous system GABA-T activity (22). Accordingly, the responses to EOS are interpreted to result from peripheral GABA-T inhibition. Body weight remained similar among EOS, vigabatrin, and saline injected mice (Fig. 5A). 4 days of EOS or vigabatrin treatment decreased serum insulin and glucose concentrations and increased the glucose:insulin ratio relative to pre-treatment (Figs. 5B-5D). 2 weeks washout from EOS or vigabatrin returned serum insulin and the glucose:insulin ratio to pre-treatment levels in both GABA-T inhibitor treated groups, while serum glucose returned to pre-treatment concentrations in EOS treated mice (Figs. 5B-5D). 5 days of EOS treatment decreased serum glucagon compared to saline injected mice (Fig. 5E).

Glucose clearance was improved in EOS and vigabatrin treated mice on day 4 of treatment compared to saline injected mice (Figs. 5F-5G). Coincident with this improved clearance, vigabatrin decreased glucose stimulated serum insulin concentrations relative to pre-treatment, while EOS tended to decrease glucose stimulated serum insulin concentration (Fig. 5H). Two weeks washout from EOS and vigabatrin markedly increased glucose stimulated serum insulin (Fig. 5H). Both GABA-T inhibitors improved insulin sensitivity within 4 days of initiating treatment (Fig. 5I-5J).

To further assess the mechanism by which GABA-T inhibition improves glucose clearance, we measured tissue specific ^{3}H-2-deoxy-D-glucose (2DG) uptake following an oral glucose gavage on day 5

of EOS or saline treatment. EOS treatment reduced 2DG uptake by the liver (19%) and increased 2DG uptake by the soleus (22%), predominantly consisting of red muscle fibers (Fig. 5K). EOS did not affect 2DG clearance by the quadriceps femoris (quad), predominantly consisting of white muscle fibers, or gonadal white adipose tissue (WAT; Fig. 5K). Given that blood perfusion is a key regulator of insulin action and glucose clearance, we subsequently measured cGMP, a key second messenger downstream of nitric oxide signaling that regulates blood flow (23). EOS increased cGMP in the soleus (59%) but had no effect in quad (Fig. 6M). In turn, GABA-T inhibition improves blood flow to oxidative red skeletal muscles.

To determine whether oral administration of GABA-T inhibitors is a viable rout of treatment, we provided obese mice with EOS in the drinking water (3 g/L) for 4 days. As we observed with IP EOS, acute oral EOS treatment decreased serum insulin and glucose concentrations and increased the glucose:insulin ratio relative to pre-treatment values (Supplemental Figs. 4A-4C). 3 days of EOS treatment improved oral glucose tolerance and reduced glucose stimulated serum insulin concentrations (Supplemental Figs. 4D-4F). EOS improved insulin sensitivity, and after a 2 week washout mice were insulin resistant (Supplemental. 4G-4H). Importantly, in lean mice which have low hepatic GABA production, there was no effect of EOS or vigabatrin (8 mg/day) on serum insulin concentrations, glucose tolerance, or insulin sensitivity (Supplemental Fig. 5). In lean mice, GABA-T inhibition with both EOS and vigabatrin decreased glucose stimulated serum insulin, while EOS decreased serum glucose (Supplemental Figs. 5B and 5F). Given the key role of GABA-T in supporting gluconeogenesis (Fig. 7), we propose GABA-T inhibition decreases serum glucose by directly impairing hepatic glucose production independent of obesity.

The Hepatic Vagal Nerve is Essential to Improvements in Glucose Homeostasis Resulting from GABA -Transaminase Inhibition

To confirm that GABA-T inhibition improves glucose homeostasis by altering hepatocyte-vagal communication, we assessed the effect of EOS treatment in HFD induced obese hepatic vagotomized and sham operated mice. Body weight was not different between surgical groups during EOS treatment (Fig. 6A). EOS decreased serum insulin and glucose, while elevating the glucose:insulin ratio in sham mice (Figs.

6B-6D). Two weeks after stopping EOS treatment all serum parameters returned to pre-treatment levels (Figs. 6B-6D). In vagotomy mice, EOS did not affect serum insulin, but decreased serum glucose and accordingly tended to elevate the glucose:insulin ratio (Figs. 6B-6D). 2 weeks washout restored serum glucose levels and decreased the glucose:insulin ratio in vagotomized mice (Figs. 6C-6D). Since hepatic GABA production supports gluconeogenic flux (Fig. 7), we expected GABAT inhibition to decrease gluconeogenesis through direct actions at the liver. In turn, diminished hepatic glucose output explains the decrease in serum glucose during EOS treatment in hepatic vagotomized mice, an effect independent of an intact vagal nerve.

EOS treatment robustly improved oral glucose tolerance and diminished glucose stimulated serum insulin concentrations in sham mice, both of which reversed after a 2-week washout (Figs. 6E-6G). EOS had no effect on oral glucose tolerance or glucose stimulated serum insulin concentrations in vagotomized mice (Figs. 6E-6G). EOS tended to improve insulin sensitivity and decrease the insulin tolerance test area under the curve in sham mice, while having no effect in vagotomized mice (Fig. 6I-6K). Together, these data support that the effects of EOS to decrease serum insulin and improve glucose clearance in obesity are dependent on an intact hepatic vagal nerve and result from hepatic specific GABA-T inhibition.

Discussion

We report a novel mechanism by which hepatic steatosis may induce systemic insulin dysregulation, while establishing that hepatocyte GABA release is regulated by hepatocyte membrane potential. Across surgical, viral, and pharmacological mouse models we have established the key role of hepatic GABA production, release, and signaling onto the vagal nerve in the dysregulation of glucose homeostasis in obesity.

The hepatic vagal nerve acts as a conduit by which the liver communicates nutritional status to affect pancreatic insulin release. Activity of the HVAN is inversely related to insulin stimulating parasympathetic efferent nerve activity at the pancreas (5, 6). Accordingly, by inhibiting HVAN activity, the obesity induced increase in hepatic GABA release may activate β-cell insulin release, driving hyperinsulinemia (6).

Vascular perfusion of skeletal muscle plays a robust role in affecting glucose clearance. Skeletal muscle blood flow and endothelial nitric oxide signaling are both impaired in obesity, directly contributing to glucose intolerance (24, 25). Endothelial nitric oxide induces vasodilation through cGMP signaling (23). We show that GABA-T inhibition by EOS increases soleus 2DG clearance and cGMP concentrations (Figs. 5K-5L). Together, our 2DG and cGMP data propose that GABA-T inhibition increases skeletal muscle NO signaling to shift orally administered glucose clearance toward red muscle fibers, which are more insulin responsive than white fibers (26). Depending on the individual muscle, red fibers account for 30-70% of total fibers and approximately 50% of whole-body muscle fibers (27, 28). Based on the findings of Griffin and Goldspink, 1973, and Iseri et al., 1952, we expect that an obese mouse is 20-25% muscle by weight (29, 30). Because red muscle fibers constitute 10-12.5% of total body weight in an obese mouse, the 22% improvement in red fiber glucose uptake exceeds the deficit resulting from the 19% decrease in hepatic glucose clearance (Fig. 5K) and explains a potential mechanism by which EOS treatment improves oral glucose clearance (Fig. 5F).

We propose a model that mechanistically links hepatic lipid accumulation with the development of hyperinsulinemia and insulin resistance (Fig. 7). Hepatic lipid accumulation increases flux through gluconeogenesis (31) and increases the hepatic FADH:FAD and NADH:NAD ratio (Supplemental Fig. 6A). The altered hepatic redox state inhibits the conversion of succinate to fumarate in the TCA cycle and instead drives succinate to succinate semialdehyde (Fig. 7; step 1). Succinate semialdehyde serves as substrate for GABA-T mediated GABA production (Fig. 7; step 2). The α-ketoglutarate formed in this reaction accepts the ammonia group from aspartate to produce oxaloacetate and glutamate, which feeds back into the GABA-T catalyzed reaction (Fig. 7; step 3). The demand for gluconeogenic substrate and the high NADH:NAD ratio drives the carbons in oxaloacetate to malate and through gluconeogenesis. This gluconeogenic drive increases aspartate metabolism, explaining the decreased aspartate release in liver slices taken from obese mice (Fig. 4F). Thus, gluconeogenic flux and a more reduced mitochondrial redox state direct the flow of intermediate molecules in obesity resulting in elevated hepatic GABA production and increased aspartate utilization.

The ion dependence of GABA transport makes hepatocyte GABA export sensitive to changes in membrane potential. Since GABA transporters are sodium co-transporters, an increase in intracellular sodium ions and hepatocyte depolarization increase GABA export (Fig. 4G). Obesity decreases hepatic ATP content (Fig. 4D) and lowers Na^+/K^+ ATPase activity (20), providing a mechanism by which obesity depolarizes hepatocytes (9) (Fig. 2A) and encourages GABA export (Fig. 4A). In fact, type II diabetics have lower hepatic ATP concentrations, and both peripheral and hepatic insulin sensitivity is significantly correlated with liver ATP concentrations (32, 33).

Our model proposes that hepatic lipid accumulation ultimately increases hepatic GABA signaling through two separate mechanisms. First, hepatic GABA production is stimulated as a result of increased GABA-T expression (Fig. 4B) and gluconeogenic flux (Fig. 7; steps 1-3), and second, hepatic GABA release is stimulated by hepatocyte depolarization (Fig. 4G). Once exported, hepatic GABA can act at $GABA_A$ receptors on vagal afferents to induce chloride influx and decrease firing rate (34) (Fig. 7; step 4),

providing a connection between hepatic lipid accumulation and decreased HVAN activity. This model explains why gluconeogenesis and hepatocytes depolarization are essential to the development of insulin resistance and hyperinsulinemia (35). Moreover, it explains how hepatic PEPCK overexpression can drive hyperinsulinemia and decrease the glucose:insulin ratio, an indirect measure of insulin sensitivity (36).

Current anti-diabetic therapeutics largely focus on managing hyperglycemia without addressing the underlying cause of disease. Herein, we have identified therapeutic targets aimed at correcting the inherent metabolic disturbances in T2D. Strategies which decrease hepatic GABA release, maintain hepatocyte membrane potential, and ultimately manipulate HVAN signaling may provide a new therapeutic approach to treat the metabolic dysfunction of obesity and T2D.

Methods

Animals

All studies excluding those done in albumin-cre expressing mice were conducted using male wildtype C57BL/6J purchased from Jackson Laboratories or bred in-house (Bar Harbor, ME). Albumin-cre male mice were purchased from Jackson Laboratories and crossed with wildtype females to generate in-house breeding of experimental albumin-cre expressing mice ($Alb^{Cre/+}$) and sibling wildtype mice ($Alb^{+/+}$). Mice were kept on a 14-hour light/10-hour dark schedule and housed 3-5 mice per cage until 1 week prior to study initiation, at which point animals were individually housed. We conducted studies in lean chow fed mice (7013 NIH-31, Teklad WI, 3.1 kcal/g, 18% kcal from fat, 59% kcal from carbohydrate, 23% kcal from protein) at 12-16 weeks of age. Studies in diet induced obese (mice dosed intraperitoneally with GABA transaminase inhibitors and mice treated with ethanolamine-O-sulfate in their drinking water were performed after 8-10 weeks on a high fat diet (TD 06414, Teklad WI, 5.1 kcal/g, 60.3% kcal from fat, 21.3% kcal from carbohydrate, 18.4% kcal from protein; 20-26 weeks of age). For Kir2.1 studies, mice were randomly assigned to a virus treatment (Kir2.1 or eGFP expression). Studies in obese Kir2.1 expressing mice were performed at 3, 6, and 9 weeks after introduction of the high fat diet and all studies were repeated in 3 different cohorts. Kir2.1 and eGFP expressing mice weighing under 36 grams after 9 weeks of high fat diet feeding were excluded from all data. Studies in obese vagotomy and sham mice were performed after 9 weeks of high fat diet feeding. Unless fasted, mice had ad libitum access to food and water. All studies were approved by the University of Arizona Institutional Animal Care and Use Committee.

Hepatic Vagotomy Surgeries

Surgeries were performed in 12-week old male C57BL/6J mice under isoflurane anesthesia. Mice were randomly assigned to a surgical group (sham or vagotomy). A ventral midline incision through the skin and peritoneum allowed us to isolate the hepatic vagus nerve as it branched from the esophagus. In

vagotomized mice, we severed the hepatic vagal nerve, while it remained intact in sham operated mice. The peritoneum was sutured with absorbable polyglactin 910 suture and the skin with nylon suture. Mice were given a single post-operative dose of slow release formulated buprenorphine analgesic (1.2 mg/kg slow release, sub-cutaneous). We monitored food intake and body weight daily and removed sutures 7 days post-operation.

Viral Induced Channel Expression

The depolarizing channel ($PSAM^{L141F,Y115F}$-5HT3HC), originally engineered by Dr. Scott Sternsons group (10), was made by mutating the acetylcholine binding domain of a chimeric channel that included the binding domain of the α7 nicotinic acetylcholine receptor and the ion pore domain of the serotonin receptor 3a. The ligand binding domain mutations (Leu^{141} → Phe and Tyr^{115} → Phe) limited the agonist action of acetylcholine and allowed for stimulation by a pharmacologically selective effector molecule PSEM89S. The exogenous ligand PSEM89S opens the serotonin receptor 3a channel allowing Na^+, K^+, and Ca^{++} passage into the cell and membrane depolarization. AAV8 viral vectors were used for plasmid delivery in all the reported studies and were synthesized by the Penn Vector Core. Hepatic specific expression of the depolarizing channel was achieved through two different methods. First, expression of a cre-recombinase dependent depolarizing channel was driven by a globally expressed CAG promoter. LoxP sites limited expression to cre-recombinase expressing tissue, and tail vein injection of $1X10^{10}$ viral genome copies established hepatocyte expression in albumin-cre but not wildtype mice (Fig. 1A-C). Second, a separate AAV8 viral vector, induced hepatic specific expression of the same depolarizing channel by driving expression using the thyroxine binding globulin (TBG) promoter. Tail vein injection of $1X10^{11}$ viral genome copies established hepatocyte expression (Fig. 2A). The thyroxine binding globulin promoter also drove hepatic expression of the hyperpolarizing, inward-rectifier K^+ channel, Kir2.1. Tail vein injection of $1X10^{11}$ viral genome copies established hepatocyte specific expression (Fig. 4A). To confirm channel expression and tissue specificity, all viral vector plasmids encoded for enhanced green fluorescent protein (eGFP).

Electrophysiology

We performed simultaneous in vivo recordings of hepatocyte membrane potential and hepatic afferent vagal nerve firing activity in anesthetized (isoflurane) mice to directly assess the effect of hepatocyte depolarization on hepatic afferent vagal nerve activity. The abdomen was shaved and scrubbed with betadine and isopropanol before an incision through the skin and peritoneum was made to expose the internal organs. The intestines were moved to expose the liver and one lobe of the liver was secured onto a small platform to minimize movement caused by respiration. A ground electrode was secured under the skin and the hepatic vagal nerve was gently lifted onto a hook-shaped electrode attached to the positive pole of a Grass P511 AC coupled amplifier, and the signal was filtered with a bandwidth of 300-1000 Hz. The nerve and hook electrode were dried and surrounded with ice cold kwik-sil to secure placement of the hook. The hepatic vagal nerve to the right of the hook, near the esophagus was cut to eliminate efferent firing. Once the kwik-sil had set, the anesthetized mouse was bathed in 37ºC Krebs-Henseleit (KH) buffer gassed with CO2. After placement and sealing of the hook electrode, 45-60 minutes of basal nerve activity was monitored/recorded with pClamp software (version 10.2; Molecular Devices) until nerve activity stabilized, after which, we began treatments.

Simultaneously, intracellular recordings of hepatocytes were made with sharp glass electrodes (30-40 MΩ) pulled from thin-walled borosilicate glass capillary tubes (OD: 1 mm; ID: 0.78mm; Sutter Instrument Co., Novato, CA), filled with 1.5M KCl and positioned visually using a motorized 4-axis micromanipulator (Siskiyou, Grants Pass, OR). Electrical signals were conducted via an Ag–AgCl electrode connected to a headstage (Axoclamp ME-1 probe), which was in turn connected to an Axoclamp 2B amplifier. Both nerve and intracellular signals were sent to an A/D converter (Digidata 1322A, Molecular Devices, Sunnyvale, CA), digitized at 20 kHz and viewed on a computer monitor using pClamp software (version 10.2; Molecular Devices).

Before treatments were applied acceptable hepatocyte impalements were determined by an abrupt negative deflection upon penetration of the cell and a stable intracellular potential (-35 to -25 mV for mouse

hepatocytes) for at least 2 minutes. If the recording of hepatocyte membrane potential was not stable the electrode was removed and membrane potential was measured on another hepatocyte.

To assess the response to channel activation, PSEM89S ligand was bath applied (30 μM) for 45 min during recordings. In order to understand the effect of Kir2.1 channel on hepatocyte membrane potential, a 10-minute baseline measure was collected and then Barium (BaCl 50 μM) was bath applied and recording continued for 45 minutes. Barium blocks Kir2.1 mediated current, thus the change in membrane potential in response to barium indicates the degree of hyperpolarization resulting from Kir2.1 channel expression. In all electrophysiology studies mice were sacrificed by cutting the diaphragm and subsequent cervical dislocation. Tissues were collected to confirm tissue specificity of channel expression and the % of hepatocytes that were expressing the channel. All studies were performed at room temperature (25ºC).

Immunohistochemistry and Imaging

To confirm the specificity and extent of viral-induced channel expression in hepatocytes, immunohistochemistry for GFP was performed. Liver, adipose, pancreas, and skeletal muscle were collected into 4% paraformaldehyde in 0.1 M PBS (Phosphate Buffered Saline) immediately after sacrifice. After 4 h at 4°C, tissues were transferred to a 30% sucrose solution in 0.1 M PBS and kept at 4°C until tissues sunk to the bottom of the solution. Tissues were snap frozen on liquid nitrogen in OTC (Optimal Cutting Temperature; Sakura Finetek USA Inc, Torrance, CA) and stored at -80°C. We used a cryostat HM 520 (MICROM International GmbH, Walldorf, Germany) to get 10 μM thick slices which we collected onto Superfrost Plus slides. We subsequently performed immunohistochemistry for GFP. Briefly, slides were washed twice in PBS and twice in PBST (3% Trition in PBS) before being exposed to blocking solution (5% normal goat serum in PBST) for 1 h. Slides were subsequently exposed to a 1:5000 dilution of the primary antibody in blocking solution (Alexa488-conjugated rabbit anti-GFP; Life Technologies, Waltham, MA) for 3 hours at room temperature. After primary antibody incubation we washed the slides 3 times in PBST and two times in PBS prior to placing the coverslip with DAPI Fluoromount-G as the mounting medium (SouthernBiotech, Birmingham, AL). Fluorescent imaging was performed without

antibody amplification in mice administered the AAV8 that encoded for Kir2.1 and tdTomato. Images were collected by fluorescent microscopy (Leica DM5500B, Leica Microsystems, Wetzlar, Germany), captured using HCImage Live, and formatted in Image-Pro Premier 9.2. 10X magnification was used to ensure a wide field of vision and accurate assessment of degree of expression.

PSEM89S Ligand Injection Studies

All studies in virus injected mice were conducted at least 5 days post virus injection to allow for maximal channel expression. Individually housed mice were intraperitoneally injected with the ligand for the depolarizing channel (PSEM89S; 30mg/kg; 0.1mL/10g body weight) or PBS (0.1mL/10g body weight). Studies conducted in mice injected with the cre-dependent depolarizing channel virus took place at 8 am. Food was removed upon study initiation. Blood for serum insulin and glucose determination was collected from the tail vein 15 minutes following intraperitoneal injection. All mice received both saline and PSEM89S ligand injection on separate days.

Studies conducted in mice expressing the cre-independent depolarizing channel began at 1 pm following a 4 hour fast. Mice received an oral glucose gavage (2.5 g/kg) 10 minutes after intraperitoneal injection of the PSEM89S ligand or saline. 15 minutes following glucose administration (25 minutes post treatment injection), blood for serum insulin and glucose determination was collected from the tail vein. All mice received both saline and PSEM89S ligand injection on separate days. These studies were repeated in 2 cohorts.

GABA Transaminase Inhibitor Studies

Wildtype lean and obese mice were randomly divided into treatment groups and dosed daily with 8 mg of ethanolamine-O-sulfate (EOS; Sigma-Aldrich, St. Louis, MO), vigabatrin (United States Pharmacopeia, Rockville, MD) or PBS (Fig. 6 and Extended Data Fig. 5). Obese sham and vagotomy mice were dosed daily with 8 mg of EOS (Fig. 7). In all cases, basal bleeds were taken prior to initiation of an ITT. Lean mice received treatment by oral gavage (0.3mL/mouse) while obese mice were treated by

intraperitoneal injection (0.3 mL/mouse). Pre-treatment studies were conducted in the week immediately prior to beginning drug administration. Daily doses took place at 9 am each day and an oral glucose tolerance tests (OGTT) and insulin tolerance tests (ITT) were performed on the third and fourth days of treatment in lean mice, respectively. In wildtype obese mice, OGTT and ITT were performed on the fourth day of treatment in separate cohorts. On the fifth day of treatment, a methylatropine bromide injection study was performed in some cohorts while other cohorts underwent a 2DG clearance study. In sham/vagotomy mice, OGTT and ITT were performed on the 4th and 5th day of treatment, respectively. After a 2-week washout period without treatment injection, a basal bleed and bleed 15 minutes after an oral glucose gavage (2.5 mg/kg) to determine oral glucose stimulated insulin secretion were performed.

In a separate set of studies, an ITT was performed in obese mice to establish insulin resistance. Subsequently, EOS was provided ad libitum in the water (3g EOS/L; Extended Data Fig. 4) for 4 days. An OGTT and ITT were performed on days 3 and 4 of treatment, respectively. The water was then removed, and an ITT was performed 2 weeks later to establish the timing of restoration of insulin resistance after drug removal.

Liver Slice Explant Studies

Liver slices from experimental mice were incubated *ex vivo* to measure release of signaling molecules. A peristaltic pump perfusion system was used to deliver warmed KH buffer to the liver through the portal vein. Briefly, mice were anesthetized with an intraperitoneal injection of ketamine (10mg/mL) and diazepam (0.5mg/mL). Once mice were unresponsive, an incision in the lower abdomen through the skin and peritoneal membrane was made vertically through the chest along with transverse incisions on both sides to expose the liver. A 30-gauge needle was inserted into the hepatoportal vein to blanch the liver. The inferior vena cava was cut to relieve pressure in the circulatory system and allow blood to drain. The perfusion continued for several minutes at a rate of 4mL/minute until the liver was completely blanched. The liver was removed and washed in warm PBS before being sliced into 0.2 mm slices using a Thomas Sadie-Riggs Tissue Slicer. Two liver slices were taken from each mouse. Tissue slices were placed

individually into a well on a 12-well plate pre-filled with 1mL of KH buffer that had been sitting in an incubator set to 37°C and gassed with 5% CO_2. Liver slices were incubated in the initial well for 1 hour to stabilize before being transferred to a fresh well pre-filled with KH buffer. Liver slices treated with the GABAT inhibitor EOS were incubated in media contained EOS (5.3 mM) during the second hour of incubation. Liver slices incubated in reduced and low NaCl media sat in normal KH buffer (NaCl 118 mM) for the first hour and then were transferred to reduced (60 mM) or low NaCl (15 mM) KH buffers for the second hour. For the reduced and low NaCl medias, respectively, 58 and 103 mM of NaCl were replaced with 116 and 206 mM of mannitol to maintain the osmolarity of the buffer. After 1 hour in the second well, tissue and media were collected. Liver slice samples and KH media samples from both wells of each mouse were pooled. Liver slices were snap frozen in liquid nitrogen, while media was frozen and stored at -80°C for future analysis.

^{3}H-2-deoxy-D-glucose Uptake Studies

On the fifth day of EOS or PBS treatment ^{3}H-2-deoxy-D-glucose (2DG; 10uCi/mouse; PerkinElmer, Waltham, MA) was given to 4 hour fasted individually housed mice. Studies were performed in 2 cohorts on 2 different days. 2DG was given by oral gavage in a solution of glucose (2.5g/kg) and each mouse received the same dose based off the average body weight for their cohort (0.1mL/10g body weight). Mice were anesthetized by isoflurane and sacrificed by cervical dislocation 45 minutes following oral gavage. Liver, soleus, quadriceps femoris, and gonadal white adipose tissue were collected, weighed, and dissolved overnight in 1N NaOH (0.5mL/50mg tissue) at 55ºC on a shaker plate. 0.5 mL of dissolved tissue was added to 5 mL of scintillation cocktail (Ultima Gold, PerkinElmer, Waltham, MA) and disintegrations per minute (DPM) were measured using a LS 6500 Multipurpose Scintillation Counter (Beckman Coulter, Brea, CA). DPM/g tissue weight was determined for each tissue and normalized based on a correction factor calculated by the average total DPM/g for all tissues divided by the total DPM/g for all tissues of the individual mouse.

cGMP Analysis

On the fifth day of EOS or PBS treatment, mice were sacrificed and the quadricep and soleus tissue were collected and frozen on dry ice. Prior to analysis, frozen quadricep were powdered using a liquid nitrogen cooled mortar and pestle to obtain homogenous muscle samples. 15-20 mg of quadricep and the entire soleus tissue (6-12 mg) were homogenized in 200 uL of a 5% trichloroacetic acid solution. Following 15 minutes of centrifugation at 3,000xg at 4°C, supernatant was transferred to a fresh tube for analysis of muscle cGMP by enzyme-linked immunosorbent assay (ELISA; ADI-900-164, Enzo Life Sciences, Farmingdale, NY).

Glucose Tolerance Test

Oral glucose (2.5g/kg; 0.1mL/10g body weight; Chem-Impex Int'l Inc., Wood Dale, IL) was given to 4 hour fasted individually housed mice. All glucose tolerance tests began at 1 pm and glucose was measured in whole blood, collected from the tail vein, by glucometer (Manufacture # D2ASCCONKIT, Bayer, Leverkusen, Germany) at 0, 15, 30, 60, 90, and 120 minutes after glucose gavage. Blood for serum insulin (oral glucose stimulated insulin secretion; OGSIS) and glucose determination was collected from the tail vein 15 minutes following glucose administration.

Insulin Tolerance Test

Intraperitoneal insulin (0.75U/kg; 0.1mL/10g body weight; Sigma Aldrich, St. Louis, MO) was given to 4 hour fasted individually housed mice. All insulin tolerance tests began at 1 pm and glucose was measured in whole blood, collected from the tail vein, by glucometer (Manufacture # D2ASCCONKIT, Bayer, Leverkusen, Germany) at 0, 30, 60, 90, and 120 minutes after insulin injection. For the studies focused on GABAT inhibition in obese mice (Fig. 6 and 7) the intraperitoneal insulin dose was (0.5 U/kg; 0.1 mL/10g body weight).

Pyruvate Tolerance Test

Intraperitoneal sodium pyruvate (1.5g/kg; 0.1mL/10g body weight; Alfa Aesar, Ward Hill, MA) was given to 16 hour fasted individually housed mice. Mice were switched to wood chip bedding (Harlan Laboratories; Cat. # 7090 Sani-Chips) at the initiation of the fast. All pyruvate tolerance tests began at 9 am and the rise in glucose was measured in whole blood, collected from the tail vein, by glucometer (Manufacture # D2ASCCONKIT, Bayer, Leverkusen, Germany) at 0, 30, 60, 90, and 120 minutes after pyruvate injection. This is indicative of hepatic gluconeogenic potential from pyruvate.

Serum Assays

Within 2 hours of collection, blood was left to clot at room temperature for 20 minutes. Thereafter the blood was centrifuged at 3,000xg for 30 minutes at 4°C and serum was collected. Serum was stored at -80°C until metabolite and hormone analyses. Serum glucose was analyzed by colorimetric assay (Cat. # G7519, Pointe Scientific Inc., Canton MI). Serum insulin was analyzed by enzyme-linked immunosorbent assay (ELISA; Cat. # 80-INSMSU-E01,E10, Alpco, Salem, NH). Serum glucagon was analyzed by enzyme-linked immunosorbent assay (ELISA; Cat. # 10-1281-01, Mercodia, Uppsala, Sweden) from tail vein blood collected at 9 am from fed mice (Vagotomy and EOS studies) or after a 4 hour fast at 1 PM (Kir2.1 study).

Explant Media Analysis

Preliminary media samples were sent to the Mayo Clinic Metabolomics Regional Core for mass spectrophotometry analysis using their neuromodulators panel (Extended Data Table 1). For all liver slice GABA and aspartate release data , we thawed the media collected from the *ex vivo* hepatic slice culture on ice and centrifuged for 5 minutes at 10,000xg at 4°C to remove tissue debris. We then measured GABA in the supernatant using a commercially available ELISA (REF# BA E-2500, Labor Diagnostika Nord, Nordhorn, Germany).

Aspartate release was measured using liquid chromatography-mass spectrometry. Samples were prepared for analysis by LC-MS/MS using protein precipitation. Twenty µl of each sample and standard curve increment was transferred to 1.5 ml tubes. One hundred eighty µl acetonitrile (ACN) was added to each tube followed by a 5 second vortex. All samples were incubated at 4°C for one hour for precipitation. Samples were then centrifuged at 10,000 RPM for 10 minutes and the supernatant transferred to 300 µl HPLC vials for analysis. The aqueous portion of the mobile phase was buffered using 10 mM ammonium bicarbonate with the pH adjusted to 7.4 using 1M formic acid and ammonium hydroxide. Methanol was used as the organic portion of the mobile phase. The column for separation was a Phenomenex Luna Silica(2) with 5 µm particle diameter and 100 Å pore size. Column internal diameter was 4.6 mm and length was 150 mm. A Shimadzu LC10 series HPLC with two dual piston pumps was used for sample injection and solvent delivery. The flow rate was fixed at 300 µl per minute. Aspartate was quantified using an LTQ Velos Pro mass spectrometer. Eluate from the Shimadzu HPLC was ionized using a Thermo ESI source. Source voltage was 6 kV; sheath and auxiliary gas flows were 40 and 20 units respectively. The ion transfer capillary was heated to 300°C. The LTQ Velos Pro was operated in negative SRM mode using two transitions: 132.1->115 for quantification and 132.1->88.1 as a qualifier. Data integration and quantification were performed using the Thermo Xcalibur software packaged with the LTQ Velos Pro.

Liver Analyses

Prior to analysis, frozen livers were powdered using a liquid nitrogen cooled mortar and pestle to obtain homogenous liver samples. To measure liver DNA content (ng dsDNA/g tissue), 10-20 mg of powdered liver was sonicated in 200µL DEPC H_2O and dsDNA determined by fluorometric assay (Cat. # P7589, Invitrogen, Waltham, MA). Whole liver mRNA was isolated from powered liver samples with TRI Reagent® (Life Technologies, Grand Island, NY) and phenol contamination was eliminated by using water-saturated butanol and ether as previously described (37). cDNA was synthesized by reverse transcription with Verso cDNA synthesis kit (Thermo Scientific, Inc., Waltham, MA), and qPCR performed using SYBR 2X mastermix (Bio-Rad Laboratories, Hercules, CA) and the Biorad iQ^{TM}5 iCycler (Bio-Rad Laboratories,

Hercules, CA). Expression of β-actin (ACTβ) and GABA-Transaminase (ABAT) mRNA were measured using the following primers (5'→3'): ACTβ; Forward – TCGGTGACATCAAAGAGAAG Reverse – GATGCCACAGGATTCCATA, ABAT; Forward – CTGAACACAATCCAGAATGCAGA Reverse - GGTTGTAACCTATGGGCACAG. LinReg PCR analysis software was used to determine the efficiency of amplification from raw output data (38). ACTβ served as the reference gene for calculating fold change in gene expression using the efficiency$^{-\Delta\Delta Ct}$ method (39).

Total liver lipids were extracted from powdered liver samples. Briefly, 10-20 mg of sample was sonicated in 100µL PBS. 1 mL of 100% ethanol was added to each sample and vortexed for 10 minutes. Following 5 minutes of centrifugation at 16,000xg at 4°C, supernatant was transferred to a fresh tube for analysis of liver triglycerides (Cat. # T7531, Pointe Scientific Inc., Canton, MI).

Hepatic NADH and NAD were quantified by fluorometric assay (ab176723, Abcam, Cambridge, UK). Hepatic ATP concentrations were assessed as previously described (40).

Statistics

We analyzed the data in SAS Enterprise Guide 7.1 (SAS Inst., Cary, NC), using a mixed model ANOVA for all analyses. ANOVA tests do not have a one-tailed vs. two-tailed option, because the distributions they are based on have only one tail. When comparisons between all means were required, we used a Tukey's adjustment for multiple comparisons. When comparisons of means were limited (e.g. only within a timepoint or treatment), we used a bonferonni correction for multiple comparisons. For the analysis of ITT, OGTT, and PTT repeated measures ANOVA were performed by including time point in the analysis. When applicable analyses were conducted separately for chow and HFD fed mice. In the Kir2.1 mice, which were monitored for response at 0, 3, 6, and 9 weeks, analyses were performed for each timepoint individually. For analysis of cre-dependent depolarizing channel effects (Fig. 2B-2F), analysis was performed in each genotype separately ($Alb^{cre/+}$ or $Alb^{+/+}$) and the main effect was injection (PSEM89S ligand or saline). For analysis of the studies using the thyroxine binding promoter driven ligand gated depolarizing channel (Fig. 2G-2I) we had the main effect of injection (PSEM89S ligand or saline). For the

vagotomy analyses (Fig. 1) the main effect was surgery (sham or vagotomy) and weeks on high fat diet when applicable. For the Kir2.1 analyses (Fig. 3 and Supplemental Figs. 2-3) the main effect was virus (eGFP or Kir2.1). Finally, for the studies using the GABAT inhibitors (Fig. 5 and Extended Data Figs. 4 and 5) the main effect was treatment (PBS, Vigabatrin, or EOS). For EOS treated sham and vagotomy mice (Fig. 6) the main effect was surgery (sham or vagotomy) and treatment (PBS or EOS). Pre-, during, and post-treatment measures were taken for basal glucose, insulin, and glucose stimulated insulin, thus a repeated measure analysis including time (pre-, during, or post-treatment) was performed separately within each injection or surgical treatment. For analysis of the effect of EOS on 2DG uptake and cGMP, analysis was performed separately for each tissue. Linear regressions of body weight and serum insulin concentrations were performed on Kir2.1 and eGFP controls, and sham and vagotomized mice using SAS Enterprise Guide 7.1. All insulin tolerance tests are presented as a percentage of baseline glucose in main and supplemental figures, and additionally presented as raw glucose values in Supplemental Fig. 7. All graphs were generated using GraphPad Prism 7.03 (GraphPad Software Inc., La Jolla, CA).

Data Availability

The datasets generated and/or analyzed during the current study are available in the Mendeley data repository at a link provided in the cover letter. Datasets will be made public upon acceptance of this manuscript.

Author Contributions:

CEG – Experimental design and project conceptualization, performed experiments and wet lab analyses, wrote initial draft of manuscript, generated figures, reviewed and edited manuscript.

CH – Performed experiments and wet lab analyses, reviewed and edited manuscript.

SG – Performed experiments and wet lab analyses, reviewed and edited manuscript.

MRH – Developed electrophysiology methodology and performed experiments, reviewed manuscript.

RFF – Developed electrophysiology methodology, reviewed and edited manuscript.

BJR – Experimental design and project conceptualization, performed surgeries and experiments, analyzed statistics, reviewed and edited manuscript.

Acknowledgments: The authors wish to thank Dr. Scott Sternson at the Howard Hughes Medical Institute, Ashburn, VA., for kindly providing the PSEM89S ligand used in these studies, Ken Pendarvis at the University of Arizona for analyzing aspartate release from our *ex vivo* hepatic slice culture model by liquid chromatography-mass spectrometry, The Mayo Clinic Metabolomics Regional Core for performing the initial mass spectrophotometry analysis of media from our *ex vivo* hepatic slice culture model using their neurotransmitter panel to identify potential hepatocyte released signaling molecules, and Drs. Masoud Ghamari-Langroudi and Richard Levine for guidance on experimental models and electrophysiology.

Funding: This research was funded by the Arizona Biomedical Research Commission Early Stage Investigator Award (Award No. ADHS14-082986; BJR), Amercian Heart Association Beginning Grant In Aid (Award No. 15BGIA25090300; BJR), Arizona Biomedical Research Commisssion Investigator Grant (Award No. ADHS18-201472; BJR)

References

1. Prevention. CfDCa (2017) National Diabetes Statistics Report, 2017. *Atlanta, GA: Centers for Disease Control and Prevention, U.S. Dept of Health and Human Services*.
2. Chang Y*, et al.* (2013) Cohort study of non-alcoholic fatty liver disease, NAFLD fibrosis score, and the risk of incident diabetes in a Korean population. *Am J Gastroenterol* 108(12):1861-1868.
3. Chon YE*, et al.* (2016) The Relationship between Type 2 Diabetes Mellitus and Non-Alcoholic Fatty Liver Disease Measured by Controlled Attenuation Parameter. *Yonsei Med J* 57(4):885-892.
4. Kotronen A, Juurinen L, Tiikkainen M, Vehkavaara S, & Yki-Jarvinen H (2008) Increased liver fat, impaired insulin clearance, and hepatic and adipose tissue insulin resistance in type 2 diabetes. *Gastroenterology* 135(1):122-130.
5. Lee KC & Miller RE (1985) The hepatic vagus nerve and the neural regulation of insulin secretion. *Endocrinology* 117(1):307-314.
6. Nagase H, Inoue S, Tanaka K, Takamura Y, & Niijima A (1993) Hepatic glucose-sensitive unit regulation of glucose-induced insulin secretion in rats. *Physiol Behav* 53(1):139-143.
7. Bernal-Mizrachi C*, et al.* (2007) An afferent vagal nerve pathway links hepatic PPARalpha activation to glucocorticoid-induced insulin resistance and hypertension. *Cell metabolism* 5(2):91-102.
8. Fernandes AB, Patarrao RS, Videira PA, & Macedo MP (2011) Understanding postprandial glucose clearance by peripheral organs: the role of the hepatic parasympathetic system. *Journal of neuroendocrinology* 23(12):1288-1295.
9. Fitz JG & Scharschmidt BF (1987) Regulation of transmembrane electrical potential gradient in rat hepatocytes in situ. *The American journal of physiology* 252(1 Pt 1):G56-64.
10. Magnus CJ*, et al.* (2011) Chemical and genetic engineering of selective ion channel-ligand interactions. *Science* 333(6047):1292-1296.
11. Thierbach R*, et al.* (2005) Targeted disruption of hepatic frataxin expression causes impaired mitochondrial function, decreased life span and tumor growth in mice. *Human molecular genetics* 14(24):3857-3864.
12. Michael MD*, et al.* (2000) Loss of insulin signaling in hepatocytes leads to severe insulin resistance and progressive hepatic dysfunction. *Molecular cell* 6(1):87-97.
13. Yan Z, Yan H, & Ou H (2012) Human thyroxine binding globulin (TBG) promoter directs efficient and sustaining transgene expression in liver-specific pattern. *Gene* 506(2):289-294.
14. Ballantyne LL*, et al.* (2016) Liver-specific knockout of arginase-1 leads to a profound phenotype similar to inducible whole body arginase-1 deficiency. *Mol Genet Metab Rep* 9:54-60.
15. Johns DC, Marx R, Mains RE, O'Rourke B, & Marban E (1999) Inducible genetic suppression of neuronal excitability. *The Journal of neuroscience : the official journal of the Society for Neuroscience* 19(5):1691-1697.
16. Gathercole LL*, et al.* (2011) Regulation of lipogenesis by glucocorticoids and insulin in human adipose tissue. *PLoS One* 6(10):e26223.
17. Scherer T*, et al.* (2011) Brain insulin controls adipose tissue lipolysis and lipogenesis. *Cell metabolism* 13(2):183-194.
18. White HL (1981) Glutamate as a precursor of GABA in rat brain and peripheral tissues. *Molecular and cellular biochemistry* 39:253-259.
19. Eskandari S, Willford SL, & Anderson CM (2017) Revised Ion/Substrate Coupling Stoichiometry of GABA Transporters. *Adv Neurobiol* 16:85-116.

20. Stanimirovic J*, et al.* (2018) Regulation of hepatic Na(+)/K(+)-ATPase in obese female and male rats: involvement of ERK1/2, AMPK, and Rho/ROCK. *Molecular and cellular biochemistry* 440(1-2):77-88.
21. Qume M & Fowler LJ (1996) Effects of chronic oral treatment with GABA-transaminase inhibitors on the GABA system in brain, liver, kidney, and plasma of the rat. *Biochemical pharmacology* 52(9):1355-1363.
22. Cooper BR*, et al.* (1980) Anorexic effects of ethanolamine-O-sulfate and muscimol in the rat: evidence that GABA inhibits ingestive behavior. *Life sciences* 26(23):1997-2002.
23. Archer SL*, et al.* (1994) Nitric oxide and cGMP cause vasorelaxation by activation of a charybdotoxin-sensitive K channel by cGMP-dependent protein kinase. *Proceedings of the National Academy of Sciences of the United States of America* 91(16):7583-7587.
24. Kubota T*, et al.* (2011) Impaired insulin signaling in endothelial cells reduces insulin-induced glucose uptake by skeletal muscle. *Cell metabolism* 13(3):294-307.
25. Laakso M, Edelman SV, Brechtel G, & Baron AD (1990) Decreased effect of insulin to stimulate skeletal muscle blood flow in obese man. A novel mechanism for insulin resistance. *The Journal of clinical investigation* 85(6):1844-1852.
26. Kern M*, et al.* (1990) Insulin responsiveness in skeletal muscle is determined by glucose transporter (Glut4) protein level. *The Biochemical journal* 270(2):397-400.
27. Edgerton VR, Smith JL, & Simpson DR (1975) Muscle fibre type populations of human leg muscles. *Histochem J* 7(3):259-266.
28. Schiaffino S & Reggiani C (2011) Fiber types in mammalian skeletal muscles. *Physiological reviews* 91(4):1447-1531.
29. Iseri LT, Alexander LC, Mc CR, Boyle AJ, & Myers GB (1952) Water and electrolyte content of cardiac and skeletal muscle in heart failure and myocardial infarction. *American heart journal* 43(2):215-227.
30. Griffin GE & Goldspink G (1973) The increase in skeletal muscle mass in male and female mice. *The Anatomical record* 177(3):465-469.
31. Im SS*, et al.* (2011) Peroxisome proliferator-activated receptor {alpha} is responsible for the up-regulation of hepatic glucose-6-phosphatase gene expression in fasting and db/db Mice. *The Journal of biological chemistry* 286(2):1157-1164.
32. Schmid AI*, et al.* (2011) Liver ATP synthesis is lower and relates to insulin sensitivity in patients with type 2 diabetes. *Diabetes care* 34(2):448-453.
33. Szendroedi J*, et al.* (2009) Abnormal hepatic energy homeostasis in type 2 diabetes. *Hepatology* 50(4):1079-1086.
34. Yuan CS, Liu D, & Attele AS (1998) GABAergic effects on nucleus tractus solitarius neurons receiving gastric vagal inputs. *J Pharmacol Exp Ther* 286(2):736-741.
35. Gomez-Valades AG*, et al.* (2008) Pck1 gene silencing in the liver improves glycemia control, insulin sensitivity, and dyslipidemia in db/db mice. *Diabetes* 57(8):2199-2210.
36. Valera A, Pujol A, Pelegrin M, & Bosch F (1994) Transgenic mice overexpressing phosphoenolpyruvate carboxykinase develop non-insulin-dependent diabetes mellitus. *Proceedings of the National Academy of Sciences of the United States of America* 91(19):9151-9154.
37. Krebs S, Fischaleck M, & Blum H (2009) A simple and loss-free method to remove TRIzol contaminations from minute RNA samples. *Anal Biochem* 387(1):136-138.
38. Ramakers C, Ruijter JM, Deprez RH, & Moorman AF (2003) Assumption-free analysis of quantitative real-time polymerase chain reaction (PCR) data. *Neuroscience letters* 339(1):62-66.
39. Livak KJ & Schmittgen TD (2001) Analysis of relative gene expression data using real-time quantitative PCR and the 2(-Delta Delta C(T)) Method. *Methods* 25(4):402-408.

40. Geisler CE, Hepler C, Higgins MR, & Renquist BJ (2016) Hepatic adaptations to maintain metabolic homeostasis in response to fasting and refeeding in mice. *Nutr Metab (Lond)* 13:62.

Main Figure Titles and Legends

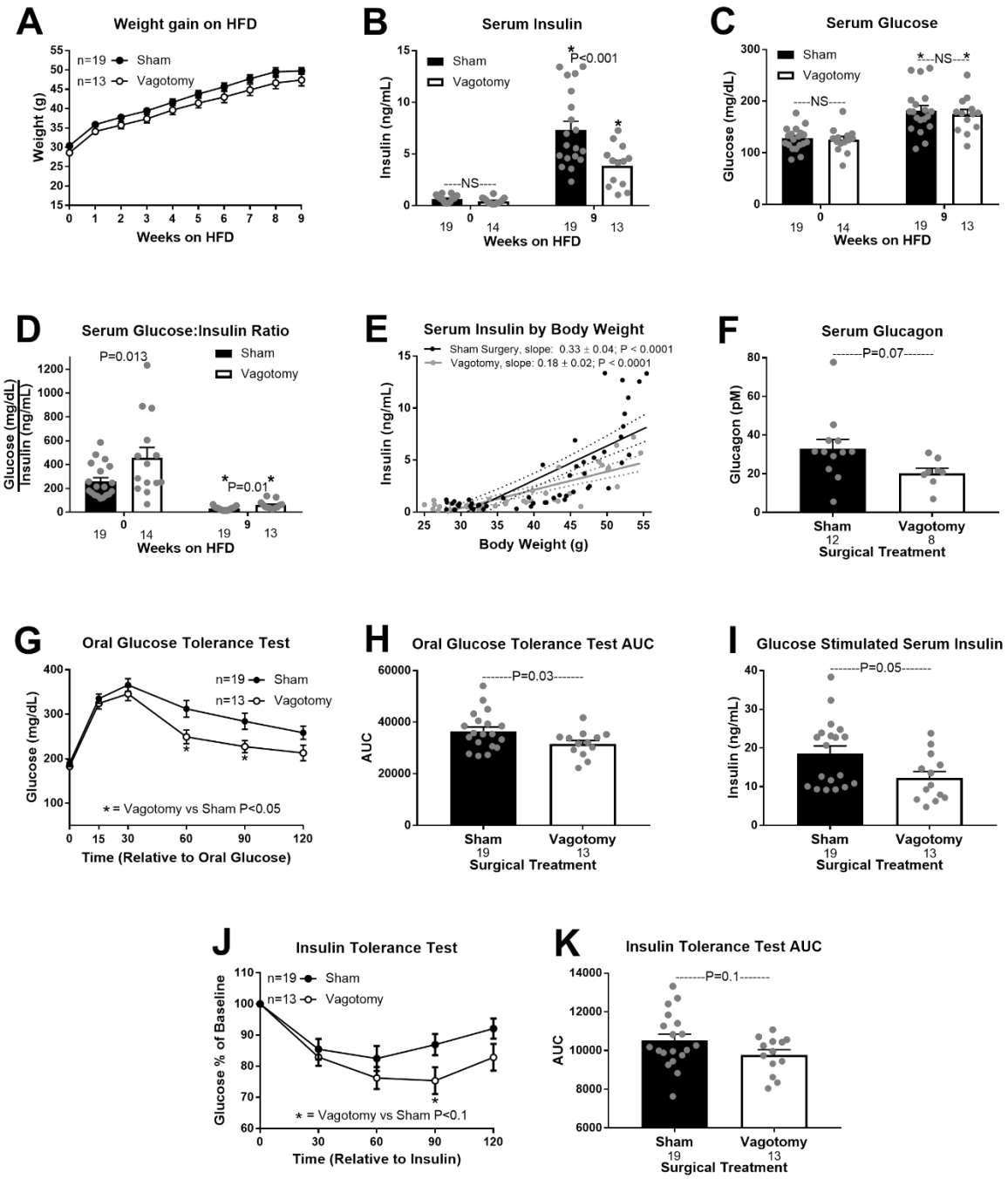

Figure 1. Hepatic vagotomy protects against diet-induced hyperinsulinemia. Effects of hepatic vagotomy on high fat diet (HFD) induced weight gain (A), serum insulin (B), glucose (C), and glucose:insulin ratio (D) at 0 and 9 weeks. (B-D) * denotes significance ($P < 0.05$) between bars of the same color. Regression of body weight and serum insulin concentrations during HFD feeding in sham and vagotomized mice (E). Effect of hepatic vagotomy after 9 weeks of HFD feeding on serum glucagon (F), oral glucose tolerance (OGTT; G), OGTT area under the curve (AUC; H), oral glucose stimulated serum insulin (I), insulin

tolerance (ITT; J), and ITT AUC (K). NS = non-significant. Number below bar denotes n per group. All data are presented as mean ± SEM.

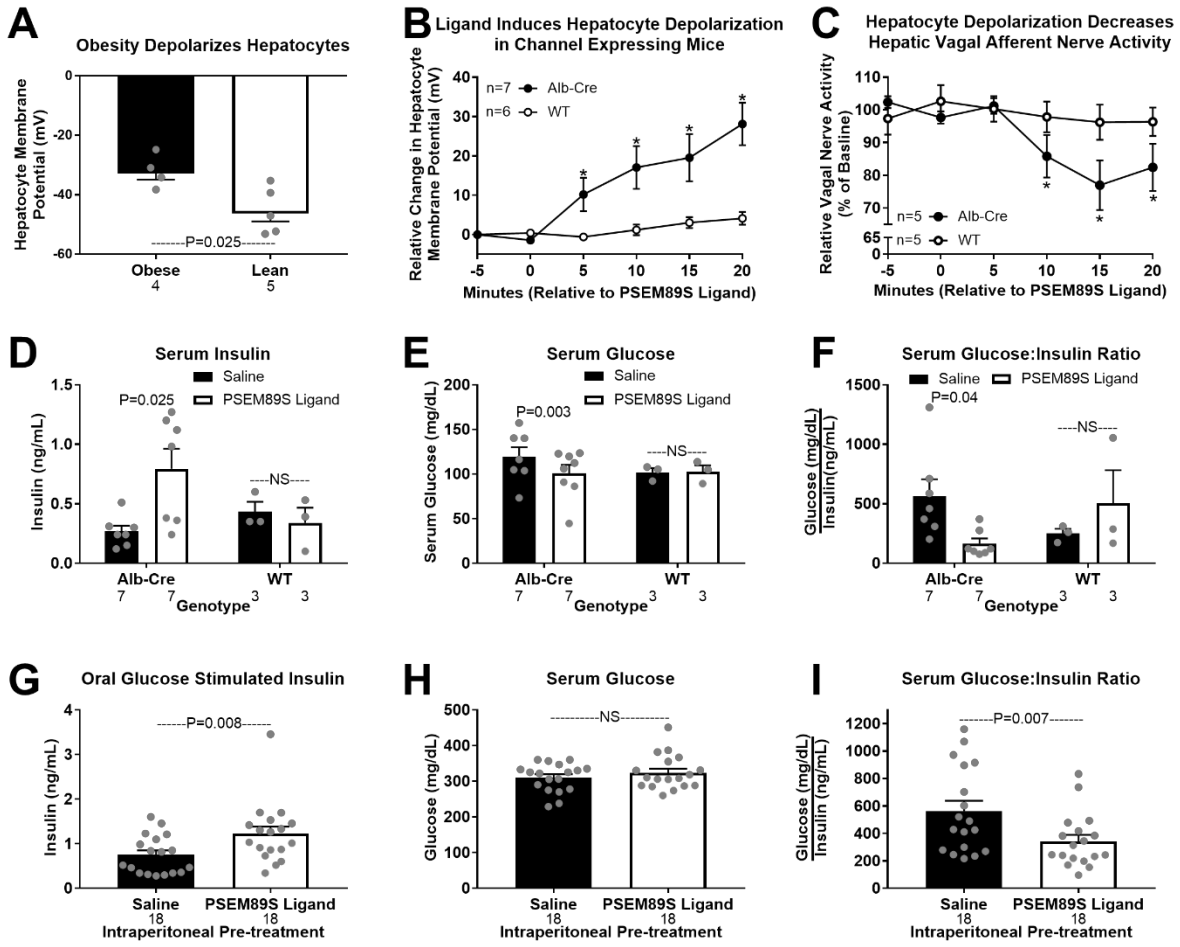

Figure 2. Acute hepatocyte depolarization depresses hepatic vagal afferent nerve activity and elevates serum insulin. Hepatocyte membrane potential in lean and obese mice (A). (B-F) Data from albumin-cre and wildtype mice tail-vein injected with an AAV8 encoding liver specific expression of the PSEM89S ligand activated depolarizing channel whose expression is dependent on cre-recombinase. PSEM89S ligand (30 μM) induced change in hepatocyte membrane potential (B). PSEM89S ligand induced relative change in hepatic vagal afferent nerve activity (C). Data in panel C was collected concurrently with data in panel B. Serum insulin (D), glucose (E), and glucose:insulin ratio (F) in albumin-cre and wildtype virus injected mice 15 minutes after saline or PSEM89S ligand (30 mg/kg) administration. (G-I) Data from wildtype mice tail-vein injected with an AAV8 encoding the PSEM89S ligand activated depolarizing channel whose liver specific expression is driven by the thyroxine binding globulin (TBG) promoter. Serum insulin (G), glucose (H), and glucose:insulin ratio (I) in channel expressing mice injected with either saline or PSEM89S ligand (30 mg/kg) 10 minutes prior to an oral glucose load (2.5 g/kg). Alb-Cre = albumin-cre, WT = wildtype, NS = non-significant. * Denotes significance ($P < 0.05$) between groups within a time point. Number below bar denotes n per group. All data are presented as mean ± SEM.

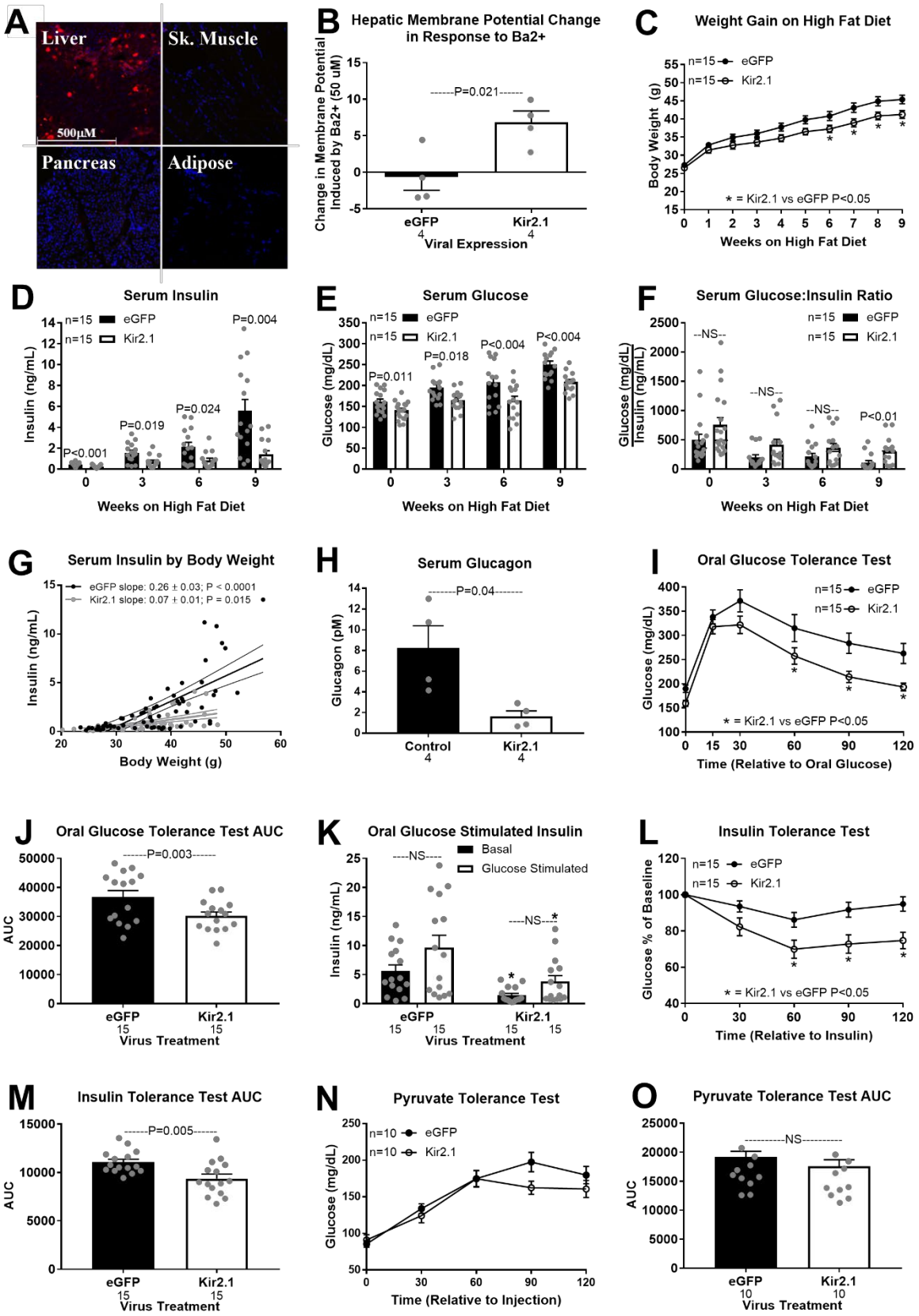

Figure 3. Hepatic hyperpolarization protects against diet-induced metabolic dysfunction**.** Liver specific expression of the Kir2.1 hyperpolarizing channel in a wildtype mouse (A). Fluorescent imaging for red = tdTomato and blue = DAPI (nucleus). Barium (BaCl; 50 μM) induced change in hepatocyte membrane potential in Kir2.1 and eGFP (control) expressing mice (B). Hepatic Kir2.1 expression effect on high fat diet (HFD) induced weight gain (C), serum insulin (D), glucose (E), and glucose:insulin ratio (F) at 0, 3, 6, and 9 weeks. Regression of body weight and serum insulin concentrations during HFD feeding in Kir2.1 and eGFP mice (G). Effect of hepatic Kir2.1 expression after 9 weeks of HFD feeding on serum glucagon (H), oral glucose tolerance (OGTT; I), OGTT area under the curve (AUC; J), oral glucose stimulated serum insulin (K; * denotes significance ($P < 0.05$) between bars of the same color), insulin tolerance (ITT; L), ITT AUC (M), pyruvate tolerance (PTT; N), and PTT AUC (O). NS = non-significant. Number below bar denotes n per group. All data are presented as mean ± SEM.

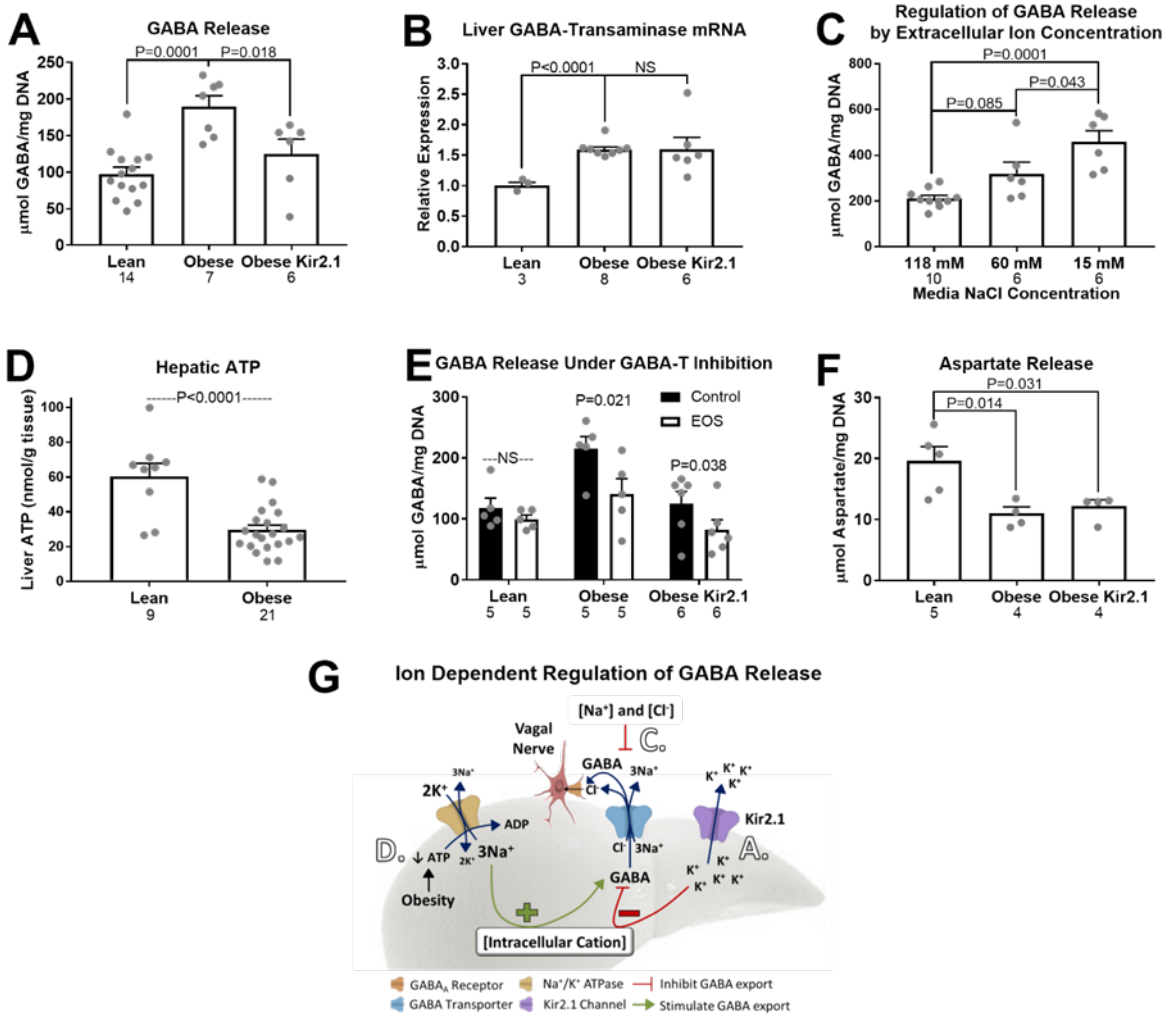

Figure 4. Hepatocyte communication with the hepatic vagal afferent nerve. Release of GABA (µmol/mg DNA) from hepatic slices (A), hepatic GABA-Transaminase (GABA-T) mRNA expression (B), release of GABA (µmol/mg DNA) from hepatic slices in normal (118 mM), reduced (60 mM), and low (15 mM) NaCl media (C), hepatic ATP (nmol/g tissue; D), release of GABA (µmol/mg DNA) from hepatic slices incubated in media containing the GABAT inhibitor, EOS (5.3 mM; E), and release of aspartate (µmol/mg DNA) from hepatic slices (F). Proposed regulation of hepatic GABA release by intracellular and extracellular ion concentrations (G). Letters within the schematic correspond with data presented in the panels above. GABA is co-transported with $3Na^+$ and $1Cl^-$ ions, so an increase in intracellular cation concentration (hepatocyte depolarization) encourages GABA export, while a decrease in intracellular cation concentration (hepatocyte hyperpolarization) limits GABA export. Kir2.1 expression induces hepatic K^+ efflux and hyperpolarization, inhibiting GABA export (G:A). Obesity decreases hepatic ATP concentrations (G:D), impairing activity of the Na^+/K^+ ATPase pump and increasing intracellular Na^+ concentrations which drives GABA export. This mechanism explains how hepatic lipid accumulation increases hepatic GABA release. Increasing extracellular NaCl concentrations inhibits GABA export (G:C). NS = non-significant. Number below bar denotes n per group. All data are presented as mean ± SEM.

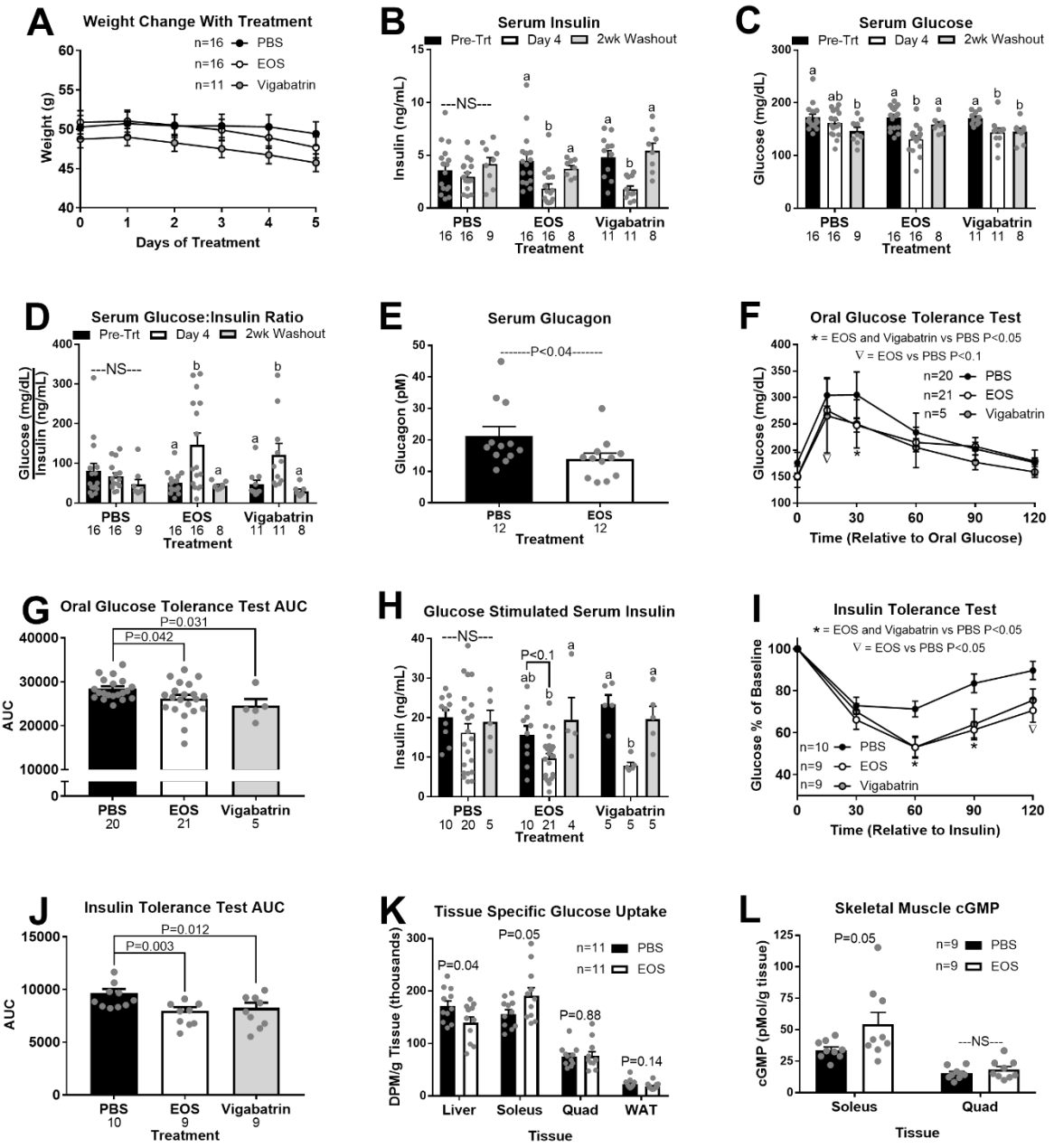

Figure 5. GABA-Transaminase inhibition improves glucose homeostasis in obesity. High fat diet induced obese mice were treated with GABA-Transaminase inhibitors ethanolamine-O-sulfate (EOS) or vigabatrin (8mg/day), or phosphate buffered saline (PBS; control) for 5 days. Body weight during treatment (A). Basal serum insulin (B), glucose (C), and glucose:insulin ratio (D) pre-treatment, on day 4 of treatment, and after a 2-week washout period. Serum glucagon in response to EOS (E). Oral glucose tolerance (OGTT; F), and OGTT area under the curve (AUC; G) on treatment day 4. Glucose stimulated serum insulin (H) pre-treatment, on day 4 of treatment, and after a 2-week washout period. Insulin tolerance (ITT; I) and ITT AUC (J) on treatment day 4. Tissue specific ^{3}H-2-deoxy-D-glucose (10 µCi/mouse; K) uptake and cGMP content (L) on treatment day 5. DPM = disintegrations per minute, NS = non-significant. ^{a,b} Bars that do not share a common letter differ significantly within injection treatment ($P < 0.05$; number below bar denotes n per group). All data are presented as mean ± SEM.

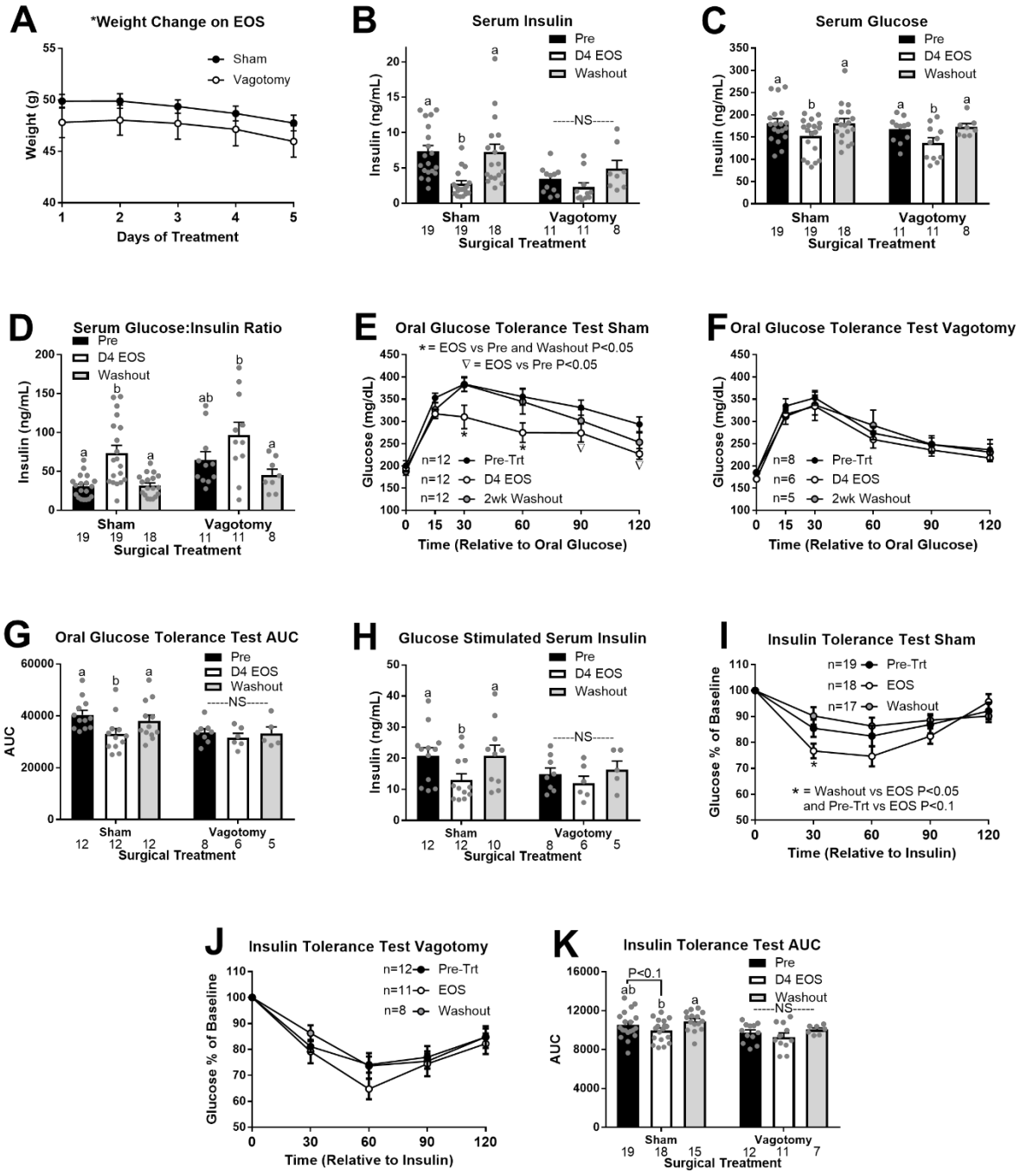

Figure 6. GABA-Transaminase inhibition improves glucose homeostasis in sham but not vagotomy mice. High fat diet induced sham operated and hepatic vagotomized mice were treated with the GABA-Transaminase inhibitor ethanolamine-O-sulfate (EOS) (8mg/day) for 5 days. Body weight during treatment (A). Basal serum insulin (B), glucose (C), and glucose:insulin ratio (D) pre-treatment, on day 5 of treatment, and after a 2-week washout period. Oral glucose tolerance in sham mice (OGTT; E), oral glucose tolerance in vagotomized mice (F) OGTT area under the curve (AUC; G), and glucose stimulated serum insulin (H) pre-treatment, on day 4 of treatment, and after a 2-week washout period. Insulin tolerance in sham mice

(ITT; I) and vagotomized mice (J), and ITT AUC (K) at pre-treatment, on day 5 of treatment, and after a 2-week washout period. NS = non-significant. [a,b] Bars that do not share a common letter differ significantly within injection treatment ($P < 0.05$; number below bar denotes n per group). All data are presented as mean ± SEM.

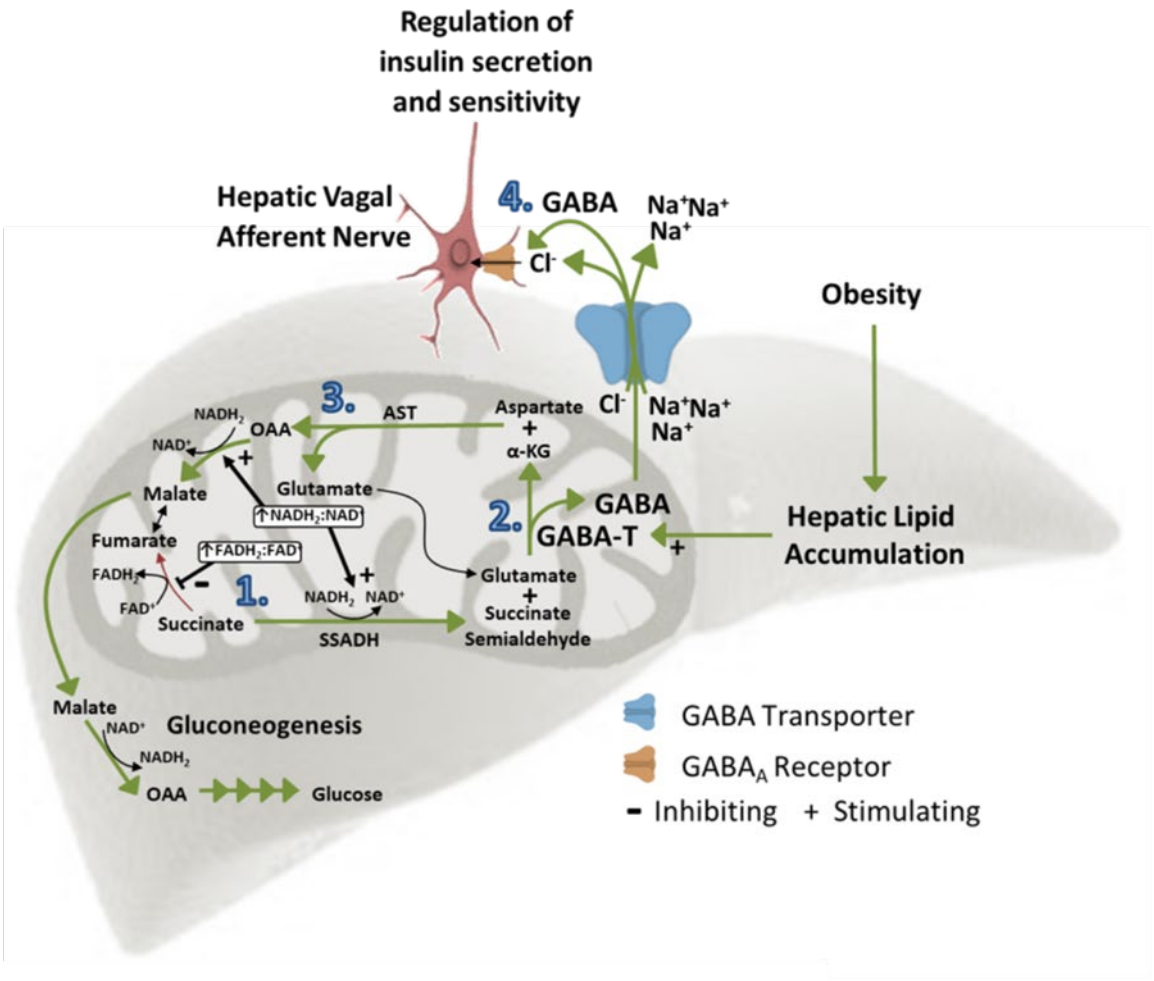

Figure 7. Working model of hepatic lipid accumulation induced changes in hepatic metabolism regulating insulin secretion and sensitivity. Obesity induced hepatic lipid accumulation depolarizes the hepatocyte resulting in a decrease in hepatic afferent vagal nerve (HVAN) activity. (1) High levels of β-oxidation in the obese liver depress the mitochondrial NAD^+:$NADH_2$ and FAD^+:$FADH_2$ ratios driving succinate to succinate semialdehyde, generating substrate for GABA-Transaminase. (2) GABA-Transaminase produces GABA and α-ketoglutarate, a substrate for aspartate aminotransferase. (3) Increased gluconeogenic flux in obesity drives the mitochondrial export of OAA as malate, and (4) released GABA acts on $GABA_A$ receptors to hyperpolarize the HVAN. Decreased HVAN activity drives hyperinsulinemia and insulin resistance. Abbreviations: OAA = oxaloacetate, AST = aspartate aminotransferase, GABA-T = GABA-Transaminase, α-KG = α-ketoglutarate, SSADH = succinate semialdehyde dehydrogenase.

Supplemental Titles and Legends

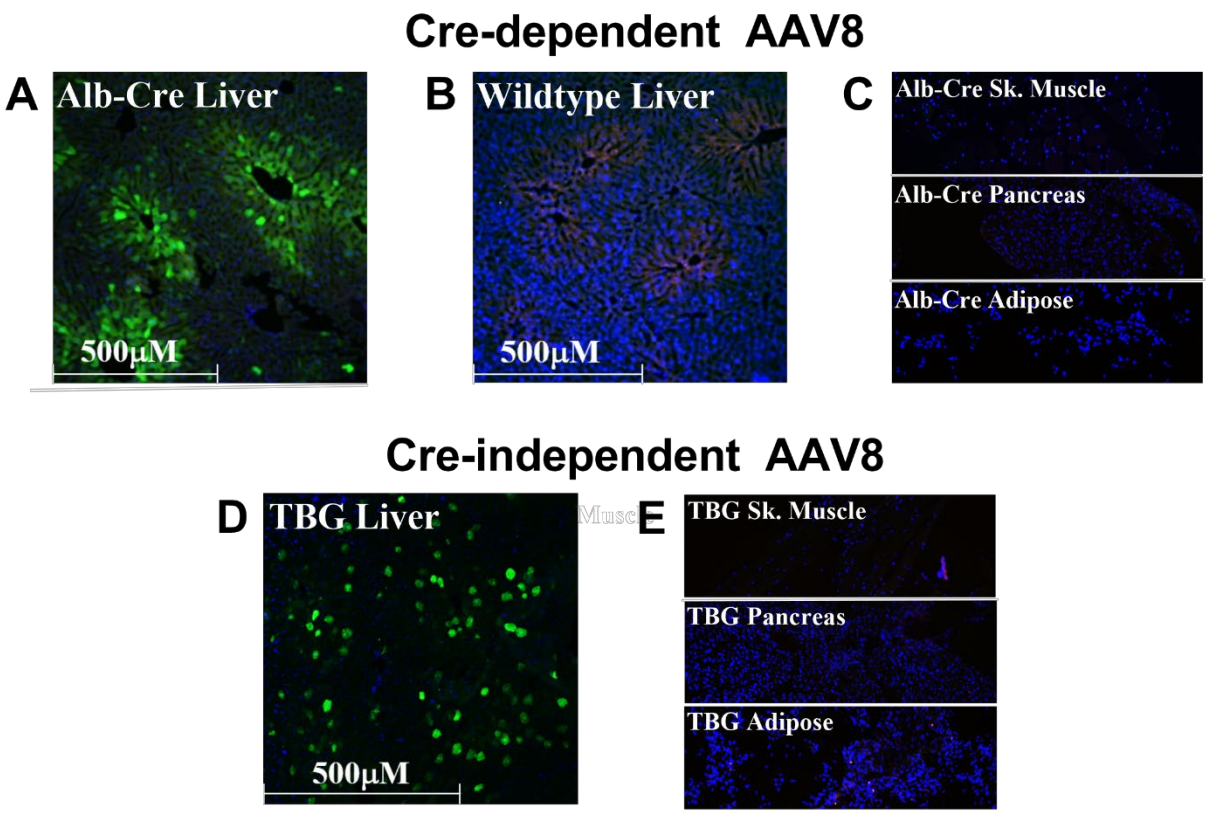

Supplemental Figure 1. Immunohistochemical validation of liver specific viral induced PSEM89S ligand gated depolarizing channel. (A-C) Liver specific expression of the PSEM89S ligand activated depolarizing channel whose expression is dependent on cre-recombinase in mice tail-vein injected with an AAV8 encoding for this channel and green fluorescent protein (GFP). Liver from an albumin-cre expressing mouse (A). Liver from a wildtype mouse (B). Skeletal muscle (Sk. Muscle), pancreas, and adipose tissue from an albumin-cre expressing mouse (C). (D-E) Wildtype mice injected with an AAV8 encoding the PSEM89S ligand activated depolarizing channel and green fluorescent protein (GFP) whose liver specific expression is driven by the thyroxine binding globulin (TBG) promoter. Liver from a wildtype mouse (D). Skeletal muscle (Sk. Muscle), pancreas, and adipose from a wildtype mouse (E). Green = GFP, blue = DAPI (nucleus), and red = background fluorescence. Alb-Cre = albumin-cre, WT = wildtype, NS = non-significant. * Denotes significance ($P < 0.05$) between groups within a time point. Number below bar denotes n per group. All data are presented as mean ± SEM.

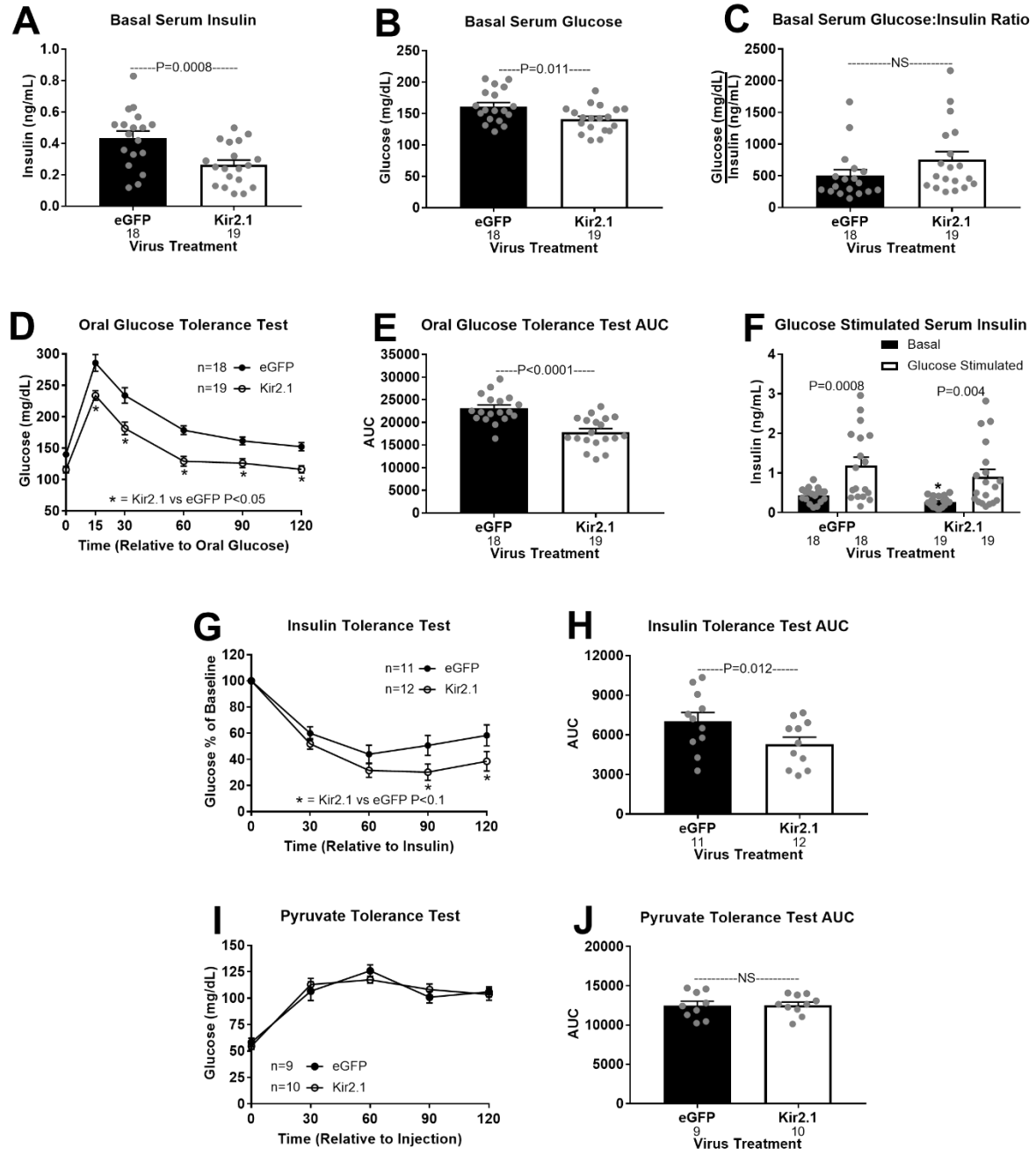

Supplemental Figure 2. Hepatic Kir2.1 expression alters glucose homeostasis in the lean mouse. Hepatic Kir2.1 expression effects on serum insulin (A) glucose (B), glucose:insulin ratio (C), oral glucose tolerance (OGTT; D), OGTT area under the curve (AUC; E), oral glucose stimulated serum insulin (F; * denotes significance ($P < 0.05$) between bars of the same color), insulin tolerance (ITT; G) ITT AUC (H), pyruvate tolerance (PTT; I), and PTT AUC (J). NS = non-significant. Number below bar denotes n per group. All data are presented as mean ± SEM.

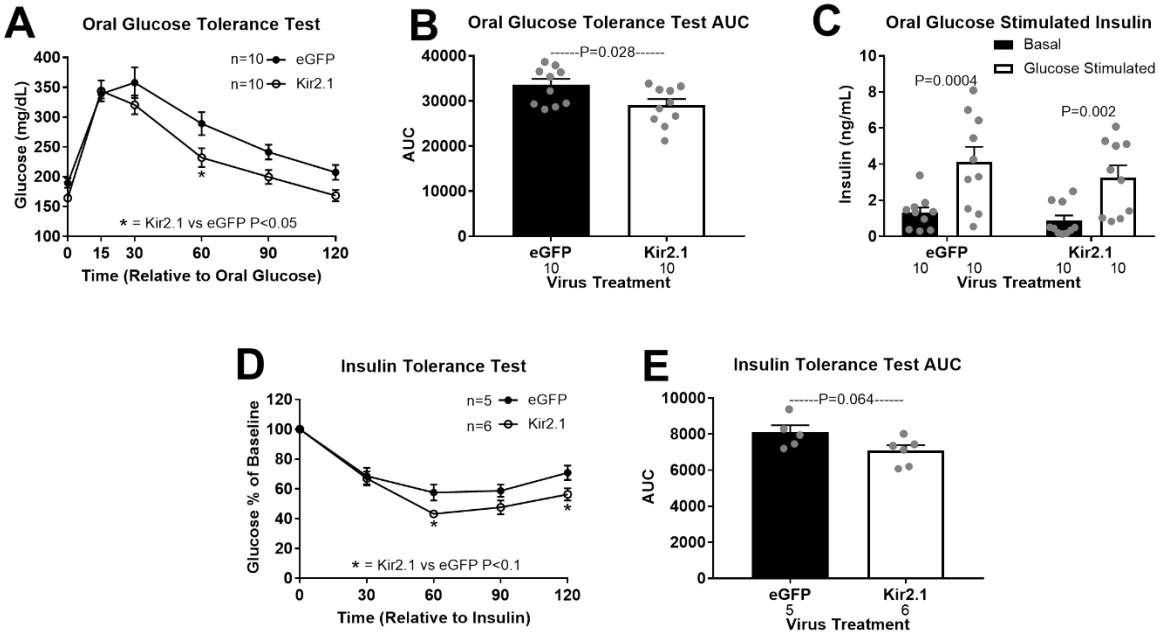

Supplemental Figure 3. Glucose homeostasis in Kir2.1 and eGFP (control) mice at 3 weeks of high fat diet feeding. Effect of hepatic Kir2.1 expression on oral glucose tolerance (OGTT; A), OGTT area under the curve (AUC; B), oral glucose stimulated serum insulin (C), insulin tolerance (ITT; D), and ITT AUC (E). NS = non-significant. Number below bar denotes n per group. All data are presented as mean ± SEM.

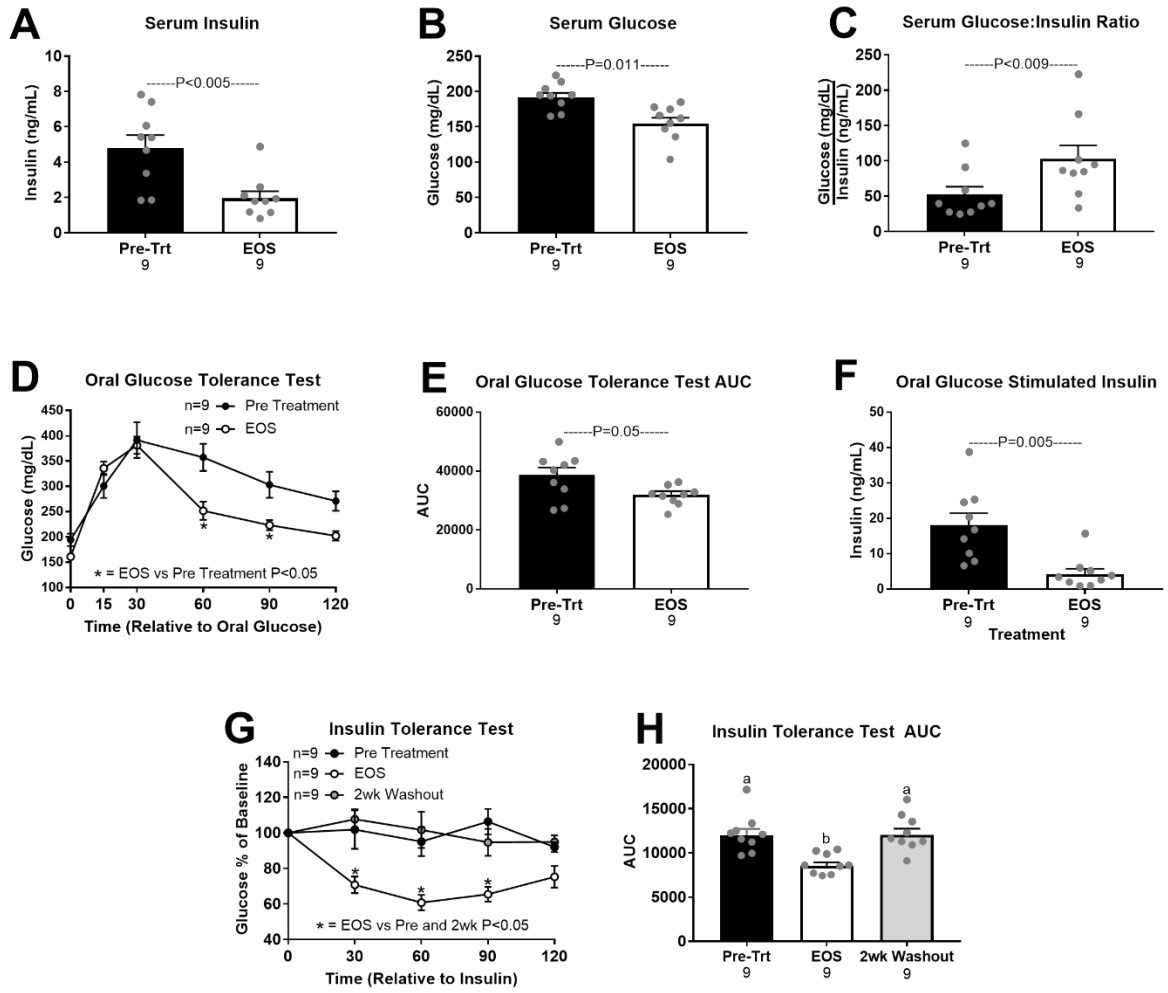

Supplemental Figure 4. Glucose homeostasis in obese male mice treated with the GABA-Transaminase inhibitor ethanolamine-O-sulfate (EOS; 3g/L in drinking water). EOS effects on serum insulin (A) glucose (B), and glucose:insulin ratio (C) pre-treatment and after 4 days of treatment. Oral glucose tolerance (OGTT; D) OGTT area under the curve (OGTT AUC; E), and oral glucose stimulated insulin (F) pre-treatment and after 3 days of treatment. Insulin tolerance (ITT; G) and ITT AUC (H) pre-treatment, on day 4 of treatment (EOS), and after a 2-week washout period. [a,b] Bars that do not share a common letter differ significantly ($P < 0.05$; number below bar denotes n per group). All data are presented as mean ± SEM.

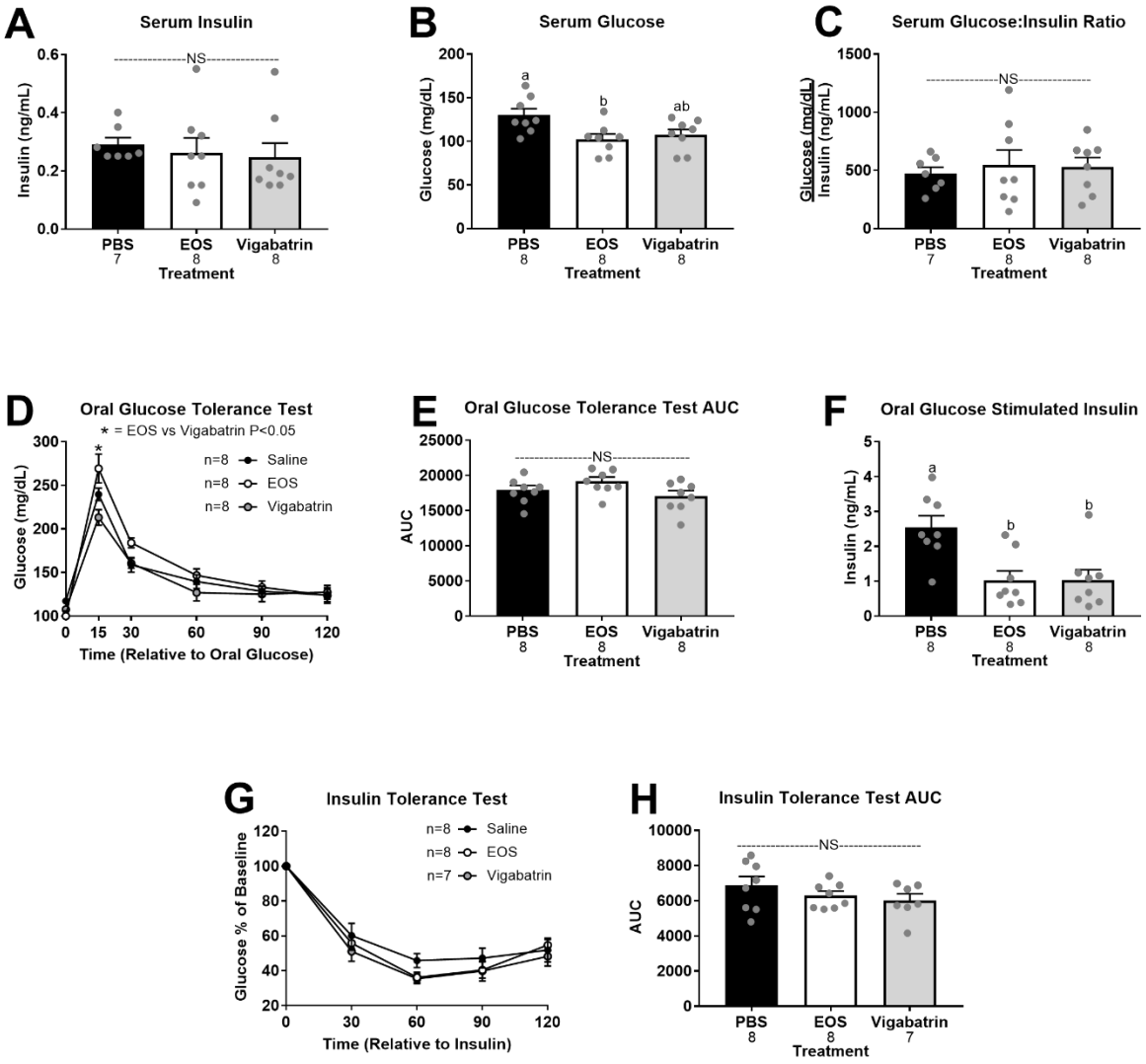

Supplemental Figure 5. Glucose homeostasis in lean male mice treated with GABA-Transaminase inhibitors ethanolamine-O-sulfate (EOS) or vigabatrin (8mg/day), or phosphate buffered saline (PBS; control). Serum insulin (A), glucose (B), and glucose:insulin ratio (C) on treatment day 4. Oral glucose tolerance (OGTT; D), OGTT area under the curve (AUC; E), and oral glucose stimulated serum insulin (F) on treatment day 3. Insulin tolerance (ITT; G) and ITT AUC (H) on treatment day 4. NS = non-significant. [a,b] Bars that do not share a common letter differ significantly ($P < 0.05$; number below bar denotes n per group). All data are presented as mean ± SEM.

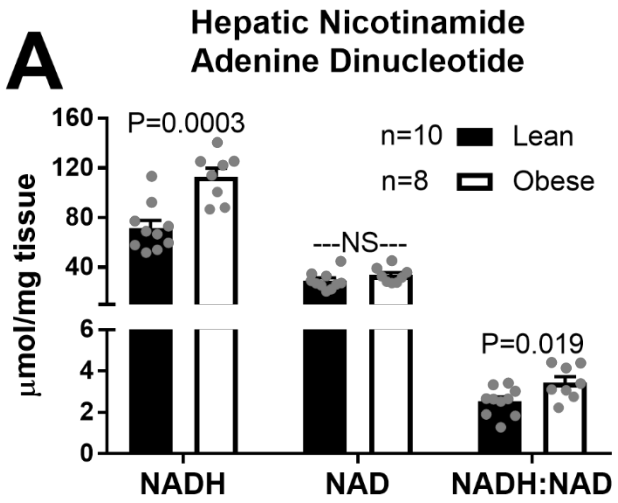

Supplemental Figure 6. Supporting data for the working model of hepatic lipid accumulation induced changes in hepatic metabolism. Hepatic nicotinamide adenine dinucleotide concentrations (A) in lean and obese mice. NS = non-significant. Number beside legend denotes n per group. All data are presented as mean ± SEM.

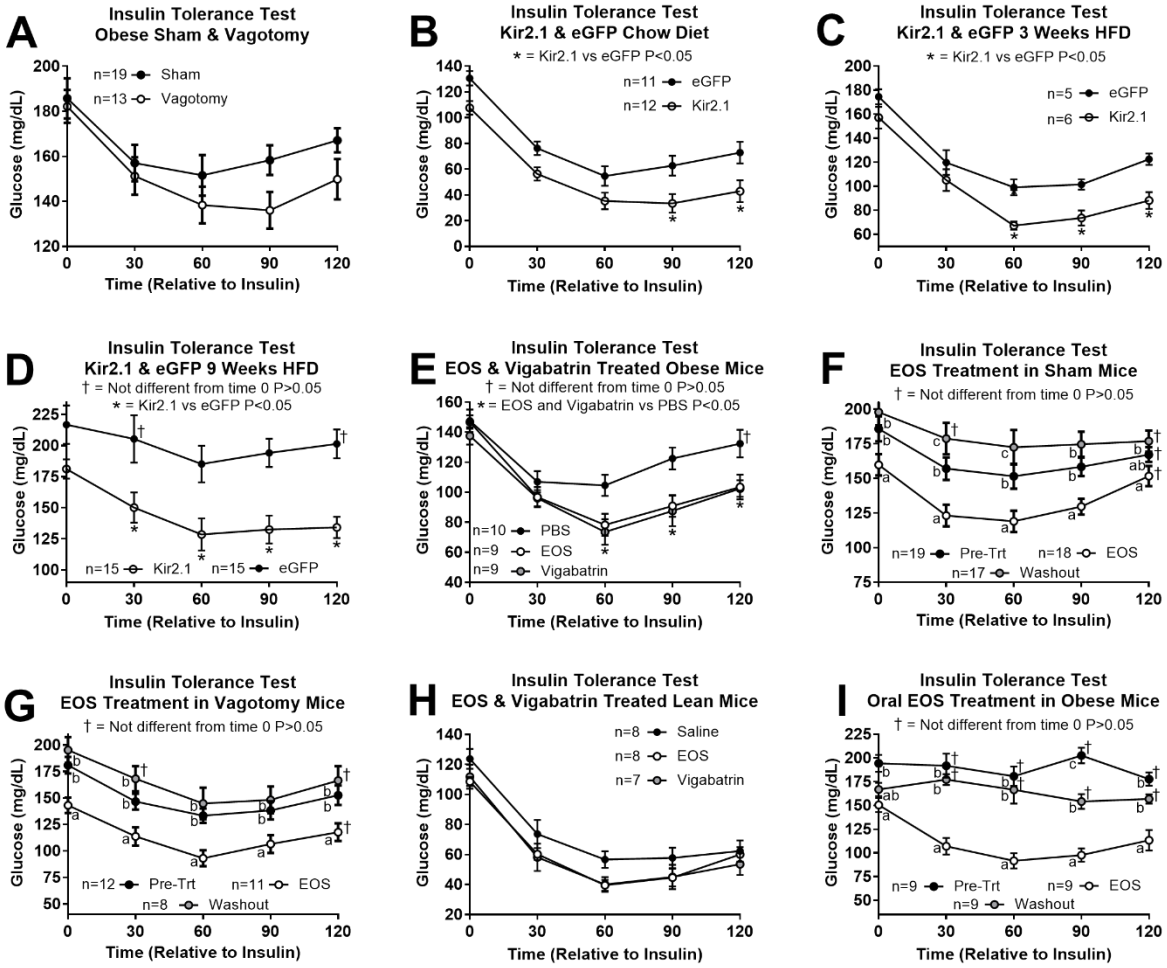

Supplemental Figure 7. Insulin tolerance tests (ITT) presented as raw glucose values. ITT in HFD fed sham and vagotomized mice (A). ITT in Kir2.1 and eGFP control mice on chow diet (B), and after 3 (C), and 9 weeks of HFD feeding (D). ITT on day 4 of EOS or Vigabatrin (8mg/day), or PBS treatment in obese mice (E). ITT in sham (F) and vagotomized mice (G) at pre-treatment, on day 5 of EOS (8mg/day) treatment, and after a 2-week washout period. ITT on day 4 of EOS or Vigabatrin (8mg/day), or PBS treatment in lean mice (H). ITT pre-treatment, on day 4 of oral EOS (3g/L in drinking water) treatment, and after a 2-week washout period. ^{a,b,c} data points that do not share a common letter differ significantly ($P < 0.05$) within a timepoint. † Denotes the data point is not significantly different from time 0 for that group ($P > 0.05$). Unless indicated, all other timepoints are significantly different from time 0 within a group of mice. * Denotes significance between groups specified in the panel within a timepoint. All data are presented as mean ± SEM.

Supplemental Table 1. Liver slice neurotransmitter panel data

Neurotransmitter (µmol/µg DNA)	Lean (N = 5)	Obese (N = 3)	% Change in Obesity
Adenosine	0.22 ±0.04	0.10 ± 0.01	-55%*
Histidine	17.74 ± 0.92	12.90 ± 0.72	-27%*
Serine	22.32 ± 3.33	13.02 ± 0.53	-42%
Taurine	238.40 ± 18.41	305.18 ± 38.04	28%
Glutamine	49.06 ± 5.19	40.39 ± 3.98	-17%
Glycine	130.74 ± 5.16	81.31 ± 4.93	-37%*
Aspartic Acid	6.92 ± 0.55	3.47 ± 0.32	-50%*
Glutamic Acid	30.32 ± 2.12	28.74 ± 3.48	-5.2%
GABA	5.43 ± 0.64	8.77 ± 0.53	61%*

Initial neuromodulators panel analysis on media collected form the liver explant studies performed by the Mayo Clinic Metabolomics Regional Core. *Indicates significant difference between obese and lean mice ($P<0.05$). Data are presented as mean ± SEM.